Megakaryocytes assemble a three-dimensional cage of extracellular matrix that controls their maturation and anchoring to the vascular niche

Claire Masson[1≠], Cyril Scandola[2≠], Jean-Yves Rinckel[1], Fabienne Proamer[1], Emily Janus-Bell[1], Fareeha Batool[1], Naël Osmani[3], Jacky G. Goetz[3], Léa Mallo[1], Nathalie Brouard[1], Catherine Léon[1], Alicia Bornert[1], Renaud Poincloux[4], Olivier Destaing[5], Alma Mansson[6], Hong Qian[6], Maxime Lehmann[1], Anita Eckly[1]

≠ First co-authors ship

[1]Université de Strasbourg, INSERM, EFS Grand Est, BPPS UMR_S1255, FMTS, F-67065 Strasbourg, France ; [2]Institut Pasteur, Université Paris Cité, Ultrastructural Bioimaging Unit, 75015 Paris, France ; [3]INSERM UMR_S1109, Tumor Biomechanics Lab, Université de Strasbourg, Fédération de Médecine Translationnelle de Strasbourg (FMTS), Strasbourg, F-67000, France. Equipe Labellisée Ligue Contre le Cancer; [4] Institut de Pharmacologie et de Biologie Structurale, Université de Toulouse, CNRS, UMR5089, 205 route de Narbonne, BP64182 31077 Toulouse, France ; [5] Institute for Advanced Biosciences, Centre de Recherche Université Grenoble Alpes, Inserm U 1209, CNRS UMR 5309, Grenoble, France; [6] Center for Hematology and Regenerative Medicine (HERM), Department of Medicine Hiddinge, Karolinska University Hospital, Karonlinska Institute, Stockholm, Sweden.

Key words : Megakaryocyte, extracellular matrice, intravasation, integrins, proteolysis

Number of figures : 7

Correspondance to: Anita ECKLY
UMR-S1255 INSERM-Université de Strasbourg
Etablissement Français du Sang-Grand Est
10, rue Spielmann, B.P. N°36
67065 Strasbourg Cedex, France
anita.michel@efs.sante.fr
Tel: (33) 388 21 25 25
Fax: (33) 388 21 25 21

30 ## Key Points

31 1. Megakaryocytes form a three-dimensional (3D) cage composed of laminin and collagen IV
32 connected to the basement membrane surrounding them. This microarchitecture stabilizes
33 megakaryocytes within their vascular niche.
34 2. β1/β3 integrins and MMP are key ECM cage regulators that assist megakaryocyte
35 maturation and intravasation at the bone marrow-blood interface.

36

Abstract

Megakaryocytes, the progenitor cells of blood platelets, play a crucial role in hemostasis by residing in the bone marrow and ensuring continuous platelet production. Unlike other hematopoietic cells, megakaryocytes do not enter the blood circulation intact. They remain anchored within the bone marrow while extending cytoplasmic protrusions called proplatelets through the sinusoidal endothelial barrier. These proplatelets subsequently fragment into functional platelets. This unique process of intravasation facilitates efficient platelet production while maintaining the megakaryocyte cell body within the bone marrow niche, thus preventing potential thrombotic complications. How the extracellular matrix (ECM) influences the delicate balance between megakaryocyte retention and proplatelet extension remains largely unknown. Here, we investigate the spatial organization and functional role of ECM components in the megakaryocyte vascular niche. Our findings reveal that laminin and collagen IV form three-dimensional (3D) ECM cages encompassing megakaryocytes and anchor them to the sinusoidal basement membrane. Gene deletion shows the existence of laminin α4 in the ECM cage that is necessary to maintain megakaryocyte-sinusoid interactions. Notably, megakaryocytes actively contribute to the ECM cage assembly; β1/β3 integrin knockout weakens these structures, increasing intravasation and entire megakaryocyte entry into circulation. The retention of megakaryocytes by these 3D ECM cages depends on dynamic remodeling processes. Inhibition of ECM proteolysis results in denser cage formation, increasing the frequence of immature megakaryocytes with impaired demarcation membrane system (DMS) development. Thus, the ECM cage represents a novel concept of an active and dynamic 3D microenvironment that is continuously remodeled and essential for maintaining megakaryocyte perivascular positioning. This specific microarchitecture guides megakaryocyte maturation and intravasation, underscoring the critical role of ECM microarchitecture and dynamics in megakaryocyte function.

INTRODUCTION

Megakaryocytes, the precursors of blood platelets, differentiate from hematopoietic stem cells and mature in a complex bone marrow microenvironment. Megakaryocytes are large, highly polyploid cells that contain a complex invaginated network of membranes, known as the demarcation membrane system (DMS), which serves as a membrane reservoir for platelet production. In contrast to other hematopoietic cells, megakaryocytes exhibit a unique platelet production process. They do not enter the bloodstream intact. Instead, they remain anchored in the bone marrow and extend cytoplasmic protrusions called proplatelets through the sinusoidal endothelial barrier. These protrusions protrude into the lumen of bone marrow sinusoids, where they undergo fragmentation to release individual platelets into the circulation. This distinctive mechanism allows for the efficient production and release of platelets while maintaining the megakaryocyte cell body within the bone marrow microenvironment, thus reducing the risk of thrombotic complications (Boscher et al., 2020; Stone et al., 2022). The remaining cell body, composed of a nucleus surrounded by a thin rim of cytoplasm, is ultimately phagocytosed in the stroma (Radley & Haller, 1983).

Megakaryocytes are strategically located at the interface between the bone marrow and the blood circulation, specifically at the parasinusoidal region (Lichtman et al., 1978; Stegner et al., 2017). Intravasation, the coordinated passage of megakaryocyte fragments through the sinusoidal barrier, requires an original, complex, and dynamic adaptation of megakaryocytes to highly different microenvironments, both mechanically and biologically. They are positioned next to the endothelial lining and its underlying basement membrane, in equilibrium between the constrained 3D environment of the bone marrow and the fluid environment of the blood. In this context, they are in contact with two types of ECM organization: basement membrane and interstitial ECM.

Megakaryocytes actively influence their structural microenvironment through several ECM remodeling mechanisms, including the endocytosis of plasma proteins like fibrinogen, and the synthesis and release of extracellular matrix (ECM) components such as fibronectin laminin, and type IV collagen (Abbonante et al., 2017; Handagama et al., 1987; Malara et al., 2014). Additionally, they produce ECM-modifying proteins, including matrix metalloproteinases (MMPs), tissue inhibitors of metalloproteinases (TIMPs), and lysyl oxidase (LOX), which facilitate the continuous renewal and regulation of the matrix (Eliades

et al., 2011; Malara et al., 2018; Villeneuve et al., 2009). Furthermore, we have recently discovered that megakaryocytes could remodel the substrate-bound fibronectin matrix into basal fibrillar structures surrounding the cells. The extent of fibrillogenesis depended on the stiffness of the substrate, and relied on both β1 and β3 integrins (Guinard et al., 2023). This intricate interplay between megakaryocytes and their surrounding ECM remodeling demonstrates the dynamic nature of the vascular niche and highlights its critical role in platelet production.

The ECM surrounding megakaryocytes plays a crucial role in their development and function. Numerous studies have identified essential components of this matrix, including collagen IV, fibronectin, fibrinogen, and laminin (Larson & Watson, 2006; Malara et al., 2014; Semeniak et al., 2016; Susek et al., 2018). The presence and function of collagen I fibers remain a subject of ongoing debate, with some researchers proposing that they guide megakaryocyte proplatelets toward sinusoids (Oprescu et al., 2022). *In vitro* studies have shown that while collagen I may inhibit proplatelet formation, other ECM components, like collagen IV, fibrinogen, and fibronectin, can facilitate this process (Balduini et al., 2008; Malara et al., 2014; Sabri et al., 2004). The diverse and sometimes contradictory roles of these ECM components in megakaryocyte behavior underscore the complexity of this research area and highlight the need for further investigation, particularly *in vivo*.

The present study provides new insight into the spatial organization of the ECM that envelops megakaryocytes, elucidating its specific architecture and molecular mechanisms governing its dynamics and function. We performed advanced 2D and 3D analyses of mouse bone marrow and identified a novel ECM cage containing laminin chains ϒ1 and α4, and collagen IV that anchored megakaryocytes to the sinusoidal basement membrane. Deleting laminin α4 impairs the connections between megakaryocytes and sinusoids. Megakaryocytes act actively in forming and maintaining this ECM cage, relying on their integrins β1 and β3. Indeed, deleting these integrins causes significant impairment of the cage's integrity, resulting in increased intravasation of megakaryocytes and an unexpected release of intact megakaryocytes into the bloodstream. Moreover, *in vivo*, matrix metalloproteinases (MMPs) inhibition reveals that dynamic ECM remodeling is crucial for maintaining the cage structure and supporting megakaryocyte development. In conclusion, our study unveils a 3D ECM cage that physically stabilizes megakaryocytes within their vascular niche. This structure facilitates

126 the physiological regulation of megakaryocyte maturation and intravasation at the bone
127 marrow-bloodstream interface.

128 ## RESULTS

129

130 *Laminin and collagen IV create a 3D cage around sinusoid-associated megakaryocytes.*

131 The organization of the ECM around megakaryocytes in the vascular niche is not well
132 understood due to challenges in *in vivo* observation. To investigate this, we utilized
133 immunofluorescence (IF) microscopy on ultrathin bone marrow cryosections (250 nm
134 thickness). This approach offers superior axial resolution compared to traditional confocal
135 microscopy, enabling high-resolution localization of ECM components. Megakaryocytes were
136 visualized using antibodies against GPIbβ, while sinusoids were identified with antibodies
137 against FABP4 (Figure 1A). Our findings revealed that laminin ϒ1 chains and collagen IV
138 delineated the basement membrane underlying the endothelium of sinusoids and the outer
139 contour of mature megakaryocytes (Figure 1A, Suppl. Figure 1Aa). Adjacent cells exhibited
140 granular staining for laminin ϒ1 and collagen IV, which may indicate a potential contribution
141 to the ECM constitution (arrow in Suppl. Figure 1Ag-h). Fibronectin was detected in the
142 basement membrane and around megakaryocytes, while fibrinogen was more widespread,
143 associated with the basement membrane, the megakaryocyte surface, and intracellular
144 granules (Suppl. Figure 1Ab-c). Von Willebrand factor (VWF) signal was restricted to the
145 alpha granules of megakaryocytes (Suppl. Figure 1Ad). We observed no detectable signals
146 for type I and III collagen around megakaryocytes or sinusoids despite using antibodies
147 validated on positive controls (Suppl. Figure 1Ae-f, Suppl. Figure 1B-C).

148 Having established the expression of laminin ϒ1, collagen IV, fibronectin, and
149 fibrinogen in the direct megakaryocyte microenvironment, their spatial organization was
150 next investigated using 3D imaging of whole-mount bone marrow preparations (Figure 1B).
151 Analysis of maximum Z-stack projections revealed that laminin ϒ1 and collagen IV formed a
152 reticular 3D ECM cage completely enveloping megakaryocytes and extending radially from
153 the sinusoidal basement membrane (Figure 1B-C). With this approach, the basement
154 membrane-ECM cage connections were clearly visible when examining the full z-stack series.
155 Examples are shown in movies 1 and 2 and in Suppl. Figures 1D-E. Quantification showed
156 that almost all megakaryocytes near sinusoids (sMK, 92.8 ± 3.3 %) have a laminin cage,
157 compared to only 11.4 ± 4.8 % of megakaryocytes in the parenchyma (pMK) (Suppl. Figure
158 1F-G). Parenchymal megakaryocytes (pMK), which represented only 18 ± 1.3 % of all

159 megakaryocyte population (Suppl. Figure 1H), were instead surrounded by a a sparse thin
160 network of laminin ϒ1 (Suppl. Figure 1F). Althought we cannot exclude that ECM cage can
161 be form on its own, our data suggests that ECM cage assembly may require interactions
162 between megakaryocytes and the sinusoidal basement membrane. Parenchymal
163 megakaryocytes (pMK), which represented only 18 ± 1.3 % of all megakaryocyte population
164 (Suppl. Figure 1H), were instead surrounded by a a sparse thin network of laminin ϒ1 (Suppl.
165 Figure 1F). The ECM cage was present at all stages of megakaryocyte maturation, including
166 megakaryocytes with proplatelet extension (Suppl. Figures 1I-J). Remarkably, after
167 mechanical dissociation and size exclusion, nearly half of the megakaryocytes successfully
168 retained their cages (53.4 ± 5.6 %, 329 megakaryocytes counted from 3 mice), indicating
169 strong physical attachments between both components (Figure 1D). While fibronectin and
170 fibrinogen are present around megakaryocytes and at the vessel-cell interface, they do not
171 form a reticular ECM cage. Furthermore, no connection was found between fibronectin and
172 fibrinogen deposition with the sinusoid basement membrane, in contrast to the findings for
173 laminin and collagen IV (Suppl. Figure 1K). These observations demonstrate that
174 megakaryocytes establish precise and tight interactions with an ECM cage made of laminin
175 ϒ1 and collagen IV in a spatially confined microenvironment at the sinusoidal basement
176 membrane.
177
178 *Reduced 3D laminin cage and vessel-associated megakaryocytes in Lamα4$^{-/-}$ mouse bone*
179 *marrow.*
180 Among the γ1 chain-bearing laminin isoforms, laminin α4 was abundantly found in bone
181 marrow sinusoid basement membrane (Susek et al., 2018). To explore the direct influence of
182 ECM organization on platelets and megakaryocytes, we utilized laminin α4-deficient mice
183 (Lamα4$^{-/-}$). These mice exhibit mild thrombocytopenia, with platelet counts approximately
184 20% lower than wild-type (WT) mice (Cai et al., 2022). Their platelets maintain a normal
185 ultrastructure and functions, as shown by flow cytometry and EM analysis (Suppl. Figures
186 2A-C). Bone marrow from Lamα4$^{-/-}$ mice showed a normal number of mature
187 megakaryocytes with characteristic ultrastructural features (Figure 2C and Suppl. Figure 2D).
188 Analysis of bone marrow explants further demonstrated that these megakaryocytes could
189 extend proplatelets, indicating preserved fundamental function (Suppl. Figures 2 E-F).

190 We next examined the ECM cage using an antibody against laminin γ1. In Lamα4$^{-/-}$ mice,
191 laminin γ1 deposition around megakaryocytes and in the sinusoid basement membrane
192 decreased by 1.7- and 2.6-fold compared to controls, indicating a disruption of the laminin
193 cage (Figures 2A-B, upper panels). However, collagen IV organization remained unaltered
194 around the megakaryocytes in these mice (Figure 2A-B, lower panels), showing that laminin
195 α4 is not necessary for collagen IV cage formation. We also analyzed megakaryocyte
196 localization in the bone marrow of Lamα4$^{-/-}$ mice (Figure 2C). The total megakaryocyte
197 density was similar to that of control mice (Figure 2D), but we observed more parenchymal
198 MK with a 1.5-fold reduction in the number of megakaryocytes near sinusoids (Figure 2E).
199 These observations highlights the role of the laminin α4 cage in maintaining optimal
200 positioning of megakaryocytes near sinusoids.
201
202 *Integrins maintain the structural properties of the ECM cages.*
203 Integrins play a crucial role in ECM remodeling. Megakaryocytes express β1 and β3
204 integrins as main ECM receptors (Yang et al., 2022). To elucidate the molecular mechanisms
205 governing the intricate interactions between megakaryocytes and the ECM cage, we
206 investigate the subcellular localization of integrins on immunostained ultrathin bone marrow
207 cryosections. Using conformation-independent antibodies, we showed the presence of β1
208 subunit at on the plasma membrane and on the DMS (Figure 3A). Similar findings were
209 obtained for total β3 integrins (Suppl. Figure 3A). In contrast, the activated form of β1
210 integrin was expressed only at interaction sites with laminin γ1 and collagen IV, suggesting
211 that activated β1 integrins mediate megakaryocyte interactions with the ECM cage (Figure
212 3B). Activated β3 integrin involvement remains to be determined, as no specific signal was
213 detected when testing two different antibodies (JonA-PE, Pac 1).
214 To test if integrin-mediated signaling plays a role in the structural assembly of the ECM
215 cage, a transgenic mouse model lacking β1 and β3 integrins in the megakaryocyte lineage
216 was used (*Itgb1*$^{-/-}$/*Itgb3*$^{-/-}$) (Figure 3C). *Itgb1*$^{-/-}$/*Itgb3*$^{-/-}$ mice were generated crossing the two
217 single loxP-flanked lines (β1$^{fl/fl}$ and β3$^{fl/fl}$ mice) with *Pf4-Cre* mice (expressing the Cre
218 recombinase under the control of the *Pf4* promoter). Our analysis revealed a 2.6-fold
219 reduction in laminin γ1 deposition on the megakaryocyte surface in *Itgb1*$^{-/-}$/*Itgb3*$^{-/-}$ mice
220 compared to *Pf4-Cre* control mice. Furthermore, intensity profiles demonstrated that
221 laminin γ1 forms a less dense network around the megakaryocytes in the double knockout

222 mice, with significantly increased mesh sizes (10.6 ± 1.3 µm vs 6.3 ± 0.6 µm, respectively)
223 (Figure 3D). Notably, this lower ECM density surrounding megakaryocytes in *Itgb1*$^{-/-}$/*Itgb3*$^{-/-}$
224 mice is not linked to increased matrix degradation or reduced laminin synthesis (Suppl.
225 Figures 3B-C). As expected, the laminin γ1 network at the basement membrane remained
226 unaffected in these mice, as the integrin deletion is restricted to megakaryocytes (Suppl.
227 Figures 3E-F).
228 Further confocal and immunoEM examination revealed a decrease in the expression of
229 fibrillar fibronectin around *Itgb1*$^{-/-}$/*Itgb3*$^{-/-}$ megakaryocytes, along with mislocalization of
230 fibrinogen in the extracellular space of the DMS instead of the granules (Suppl. Figures 3G
231 and 3H). These findings show that megakaryocytes, through β1 and β3 integrins dependant
232 mechanisms, participate in their ECM microenvironment remodelling (ECM cage and
233 fibronectin, fibrinogen deposition) and that megakaryocytes β1 and β3 integrins are
234 required.
235
236 *Normal ECM organization is essential for proper megakaryocyte intravasation.*
237 Next, we investigate the relevance of the ECM cage to platelet and megakaryocyte
238 functions. Flow cytometry showed that *Itgb1*$^{-/-}$/*Itgb3*$^{-/-}$ platelets have intact α-granule
239 secretion but impaired integrin-mediated aggregation, consistent with the bleeding
240 phenotype observed in these mice (Janus-Bell et al., 2024) (Suppl. Figure 4A). As we
241 previously described that *Itgb1*$^{-/-}$/*Itgb3*$^{-/-}$ mice had a 50% reduction in platelet count
242 (Guinard et al., 2023), we hypothesized that the organization of the ECM cage could
243 contribute to the maturation process of megakaryocytes. Firstly, the number, ploidy, and
244 maturation stages of megakaryocytes in *Itgb1*$^{-/-}$/*Itgb3*$^{-/-}$ mice are similar to control mice.
245 However, consistent with previous reports, these mutant megakaryocytes have a
246 disorganized membrane system and smaller cytoplasmic areas compared to normal cells
247 (Suppl. Figures 4B-E). We also analyzed megakaryocyte localization in the bone marrow
248 tissue. We found a significantly higher proportion of megakaryocytes that were extending
249 intravascular fragments (i.e., intravasation) in *Itgb1*$^{-/-}$/*Itgb3*$^{-/-}$ mice (15.1 ± 2.7% of total bone
250 marrow megakaryocytes) compared to that in *Pf4Cre* mice (2.9 ± 0.4% of total
251 megakaryocytes). More strikingly, intact megakaryocytes were found in the sinusoid lumen,
252 a rare phenomenon in control mice under physiological conditions (Figures 4A-B).

253 To elucidate which of the two integrins was responsible for the observed phenotype, we
254 employed single-knockout mice (Figure 4C). Analysis of the ECM cage revealed a trend
255 towards decreased laminin ϒ1 density around *Itgb1*$^{-/-}$ megakaryocytes, while no notable
256 changes were observed around *Itgb3*$^{-/-}$ cells. No statistically significant increase in
257 intravasation events was observed in either single knock-out mouse model. This suggests a
258 redundant role of both integrins in regulating the megakaryocyte ECM cage and the
259 intravasation process, potentially compensating for each other's role. Additionally, we
260 investigate the role of GPVI, one of the two well-characterized collagen receptors in this
261 process (Figure 4C), and no alterations in ECM cage formation or intravasation behavior
262 were noticed, which is in agreement with previous reports (Semeniak et al., 2019).

263 To understand the unusual localization of circulating *Itgb1*$^{-/-}$/*Itgb3*$^{-/-}$ megakaryocytes in
264 the bloodstream, we used intravital 2-photon microscopy imaging to describe the dynamic
265 of the megakaryocyte behavior. We used the GPIX marker, a subunit of the GPIb-V-IX
266 complex that is expressed on mature megakaryocytes, to track the behavior of
267 megakaryocyte in living mice. Among the stabilized megakaryocytes at the parasinusoidal
268 interface, we could observe the cellular distortions of *Itgb1*$^{-/-}$/*Itgb3*$^{-/-}$ megakaryocytes and
269 their exit of the marrow (Figures 4D-E, movie 3). Flow cytometry analysis did not allow us to
270 detect intact megakaryocytes in the blood in *Itgb1*$^{-/-}$/*Itgb3*$^{-/-}$ blood samples (Suppl. Figure
271 4F). However, large megakaryocyte nuclei were observed within the downstream pulmonary
272 capillaries of these mice (Figures 4F-G), suggesting that circulating megakaryocytes in *Itgb1*$^{-/-}$
273 /*Itgb3*$^{-/-}$ mice are in large proportion retained in lung microvasculature shortly after entering
274 the bloodstream. Transmission electron microscopy (TEM) observation confirmed that intact
275 *Itgb1*$^{-/-}$/*Itgb3*$^{-/-}$ megakaryocytes were similar in size and ultrastructure to those in the stroma
276 compartment (Figure 4H). Furthermore, no significant change in the size of the endothelial
277 pores (*Itgb1*$^{-/-}$/*Itgb3*$^{-/-}$: 4.6 ± 0.3 µm; *Pf4Cre*: 4.3 ± 0.4 µm) was observed, indicating that
278 increased megakacaryocyte intravasion in not link to endothelium alteration in mutant mice.

279 *Integrins promote megakaryocyte adhesion to the ECM components of the bone marrow*

280 We next assessed the contribution of integrins adhesive function in megakaryocyte
281 anchorage to ECM. Under static conditions, most *Itgb1*$^{-/-}$/*Itgb3*$^{-/-}$ megakaryocytes did not
282 spread and still showed a round shape on immobilized laminin, fibronectin or fibrinogen
283 (Figures 5A-B). We next measured the adhesive potential of freshly isolated bone marrow

284 megakaryocytes to test for such an adhesive role. To this end, we used a miniaturized
285 microfluidic-based experimental model in which individual megakaryocyte detachment was
286 tracked when exposed to a flow rate of 300s-1, similar to the flow typically found in
287 sinusoids (Suppl. Figure 5A-B). *Pf4-Cre* megakaryocytes had capture yields of 70.5% on
288 laminin, 83.6% on fibrillar fibronectin, and 82.0% on fibrinogen. Laminin exhibited the least
289 adhesion, emphasizing the importance of the molecular composition of the said 3D ECM
290 cage and its evident impact on the adhesion response of megakaryocytes *in vivo* (Figures 5C-
291 D). *Pf4-Cre* megakaryocytes remained anchored, while *Itgb1*$^{-}$/$^{-}$/*Itgb3*$^{-}$/$^{-}$ megakaryocytes
292 experienced higher detachment rates across various ECMs (movies 4 and 5). In line with this
293 conclusion, we used the bone marrow explant model to study the adhesion properties of the
294 megakaryocytes associated with their 3D ECM cage (Figures 5E-F). This model enabled us to
295 quantify the physical detachment of megakaryocytes at the periphery of the explants. After
296 3 hours, more megakaryocytes detached from *Itgb1*$^{-/-}$/*Itgb3*$^{-/-}$ bone marrow tissue than *Pf4-*
297 *Cre* explants, reaching a plateau at 6 h. These findings indicate that β1 and β3 integrins
298 control ECM-megakaryocyte interactions in their native bone marrow microenvironment.
299 Collectively, our results highlight the essential roles of β1 and β3 integrins in forming 3D
300 ECM cages around megakaryocytes and modulating their adhesion within the bone marrow,
301 which helps stabilize the cells in their vascular niche and prevent the passage of intact
302 megakaryocytes through the sinusoid barriers.
303
304 *Cage compression via metalloproteinase inhibition affects the maturation of*
305 *megakaryocytes.*
306 Our results suggest that a weakened ECM cage promotes megakaryocyte
307 intravasation through reduced adhesion. We, therefore, tested whether an increase in cage
308 density also may affect megakaryocyte functions. For that purpose, we proposed to
309 decrease the catabolic aspect occurring in the ECM equilibrium between its synthesis and
310 degradation. To this aim, mice were injected with batimastat (30 mg/kg) and ilomastat (20
311 mg/kg) for 7 days, in order to inhibit the activation of MMPs in the megakaryocyte
312 microenvironment (Winer et al., 2018) (Supplemental Figure 6A). These mice produced
313 platelets normally in terms of both count and average platelet function (Suppl. Figures 6B-C).
314 Regarding the cage, this treatment increased the ECM density in megakaryocyte
315 surrounding, as evidenced by reduced fiber length and pore size (Figures 6A-B).

316 We investigated whether this denser ECM cage might affect megakaryopoiesis.
317 Remarkably, treatment with MMP inhibitors resulted in a significantly higher proportion of
318 smaller megakaryocytes compared to untreated mice (white arrows in Figures 6C-D). To
319 better evaluate the extent of this defect, we employed TEM (Figure 6E). We found that 53.7
320 % of the megakaryocytes lacked the appropriate organization of the DMS in MMP inhibitors-
321 treated mice, reflecting a primary failure in the cytoplasmic maturation (Stage II in Figure 6F
322 right). To determine whether MMP inhibition could directly affect megakaryocytes, we
323 cultured primary megakaryocytes in the presence of increasing concentrations of inhibitors.
324 We found no significant change in their proliferation, maturation, and proplatelet formation
325 (Suppl. Figure 6D). Although these *in vitro* system and exogenous MMPs may not fully
326 recapitulate the complexity of the bone marrow situation, these findings suggest that
327 disturbing ECM remodelling significantly impacts megakaryocyte maturation.
328 An additional phenotype associated with a denser ECM environment is a significant
329 increase in the total megakaryocyte number in MMP inhibitor-treated mice compared to the
330 control condition (Figures 6D and 6F left). Moreover, immunofluorescence analysis of bone
331 marrow sections revealed an upregulation of activated β1 integrin (Suppl. Figure 6E). These
332 results indicate that increased ECM density may promote megakaryocyte adhesion within
333 the congested microenvironment of the bone marrow. To further investigate this point, we
334 quantified the number of megakaryocytes released from bone marrow explants. We
335 observed a significant reduction in megakaryocyte egress from the bone marrow
336 microenvironment after 6 h in MMP inhibitor-treated compared to control mice (Figure 6G-
337 H). Together, these results indicate that MMPs are essential regulators of ECM homeostasis
338 within the bone marrow, influencing megakaryocyte maturation and attachment to the
339 vascular niche.
340
341

342 **DISCUSSION**

343 Physiological platelet formation relies on the strategic positioning of mature
344 megakaryocytes at sinusoids to facilitate polarised proplatelet extension and platelet release
345 into circulation. This study identifies a 3D ECM cage anchoring megakaryocytes to bone
346 marrow sinusoids. This cage, composed of laminin γ1 and α4 and collagen IV fibers, extends
347 from the basement membrane and surrounds megakaryocytes. Megakaryocyte integrin
348 signaling and ECM proteolysis regulate its remodeling and adhesive properties. This dynamic
349 microenvironment is key for megakaryocyte positioning, maturation, and intravasation into
350 the bloodstream, representing a novel concept in understanding physiological platelet
351 formation (Graphical Abstract, Figure 7).

352 In line with previous studies (Guinard et al., 2023; Larson & Watson, 2006; Malara et
353 al., 2014; Semeniak et al., 2016), we identified the presence of collagen IV, laminin γ1,
354 fibronectin, and fibrinogen surrounding sinusoid-associated megakaryocytes. Notably, when
355 analyzed using immunofluorescence and transmission electron microscopy (TEM), collagen I
356 fibers were absent under steady-state conditions. The discrepancy between our results and
357 those reported in the literature may be attributed to differences in staining methodologies
358 or variations in the physiological context of the bone marrow. Furthermore, our findings
359 indicate that GPVI-deficient megakaryocytes do not display alterations in ECM cage
360 formation, vessel association and intravasation behavior. These observations support studies
361 showing GPVI and α2β1 integrins are not critical for megakaryocyte function, underscoring
362 potential redundancy in ECM-receptor interactions (Semeniak et al., 2019). Besides, non-
363 protein ECM molecules, including glycosaminoglycans, have been shown to play an essential
364 role in supporting megakaryocyte function, including maturation (Petrey et al., 2016;
365 Piszczatowski et al., 2022; Vögtle et al., 2019).

366 We identify laminin and collagen IV as the principal structural components of this
367 ECM cage. Consistent with previous research (Abbonante et al., 2016; Cai et al., 2022; Susek
368 et al., 2018), these ECM proteins were detected intracellularly within megakaryocytes and in
369 stromal cells situated in their vicinity. This indicates that the ECM cage proteins may be
370 derived from autocrine synthesis and their production by neighbouring cells. Interestingly,
371 while fibronectin and fibrinogen were found around megakaryocytes, they do not form a
372 ECM cage, suggesting distinct functional roles, potentially related to megakaryocyte
373 expansion in bone marrow fibrosis (Malara et al., 2019; Matsuura et al., 2020).

374 Our findings in *Lamα4*-deficient mice reveal that the ECM cage is critical for
375 positioning megakaryocytes near sinusoids. It is established that CXCL12 is a most potent
376 physiological chemoattractant for megakaryocytes and that the parasinusoidal location of
377 megakaryocytes in the bone marrow is mediated by the CXCL12/CXCR4 interaction (Hamada
378 et al., 1998; Wang et al., 2019). Other chemoattractive factors also include fibroblast growth
379 factor 4 (FGF4) (Avecilla et al., 2004) and VWF (Ouzegdouh et al., 2018). Besides its potential
380 role as a reservoir of such growth factors, we show that the ECM cage is also a crucial
381 element in maintaining megakaryocytes in the proximity of sinusoids, which is essential for
382 their efficient maturation and optimal platelet production. We also find the persistent
383 presence of this ECM cage throughout megakaryocyte maturation, supporting previous
384 findings that megakaryocyte development occurs primarily at the sinusoid (Gaertner et al.,
385 2024; Lichtman et al., 1978; Stegner et al., 2017).
386 Our study highlights the indispensable roles of β1 and β3 integrins in maintaining
387 megakaryocyte stability within the vascular niche. We demonstrate that these integrins are
388 crucial for two fundamental processes : (1) the building of the 3D ECM cages, and (2) the
389 ECM-mediated adhesion mechanisms to the vascular niche. Integrins biochemical and
390 mechanical signal transduction play key roles in ECM remodelling (Larsen et al., 2006) and
391 can generate the forces that may cause these changes (Lemmon et al., 2009). For instance,
392 RhoA inhibition in *Itgb1*$^{-/-}$/*Itgb3*$^{-/-}$ megakaryocytes (Guinard et al., 2023) is likely
393 contributing to the altered ECM remodeling. Nevertheless, we still need to understand how
394 in megakaryocyte β1 or β3 integrins participate in ECM remodelling and ECM cage dynamics.
395 Our work further demonstrates that in these mice, intact megakaryocytes can enter the
396 general circulation. Of note, no intravascular megakaryocytes were found in *Lamα4*-deficient
397 mice, which have a normal collagen IV cage but a compromised laminin cage. This indicates
398 that integrity of all components of the cage is not needed to keep megakaryocytes from
399 entering circulation. Importantly, circulating megakaryocytes have also been observed in
400 humans during emergency megakaryopoiesis, such as in cases of infectious diseases,
401 inflammatory conditions, and following cardiopulmonary bypass procedures (Frydman et al.,
402 2023; Gelon et al., 2022; Puhm et al., 2023; Rapkiewicz et al., 2020). These circulating
403 megakaryocytes have been implicated in thrombotic complications, underscoring the
404 importance of integrin signaling-dependent mechanisms regulating megakaryocyte retention
405 and release.

The precise role of the ECM cage in platelet production remains incompletely understood. In the Lamα4^{-}/$^{-}$ mice, a collagen-rich ECM cage persists with normal fibronectin deposition, whereas the *Itgb1*$^{-}$/$^{-}$/*Itgb3*$^{-}$/$^{-}$ model displays a much more severe phenotype, characterized by the loss of both the laminin cage and collagen, along with the absence of fibrillar fibronectin. The preserved collagen and fibronectin in Lamα4^{-}/$^{-}$ mice may allow for residual activation of signaling pathways - potentially through integrins or alternative mechanisms - compared to the *Itgb1*$^{-}$/$^{-}$/*Itgb3*$^{-}$/model, where these matrix components are absent.

MMPs profoundly influence megakaryocyte maturation and their association with the vascular niche by modulating the density of ECM cage architecture. This finding highlights the dynamic nature of the bone marrow microenvironment and its impact on megakaryopoiesis. Dysregulation of ECM production, often associated with bone marrow pathologies, can lead to its uncontrolled accumulation. In myelofibrosis, for instance, megakaryocytes secrete transforming growth factor-β1 (TGF-β1) which stimulates excessive ECM production by stromal cells (Abbonante et al., 2016). This pathological ECM accumulation leads to abnormally smaller megakaryocytes that exhibit reduced platelet production (Gianelli et al., 2023; Malara et al., 2018; Sarachakov et al., 2023). Likewise, we observed smaller and immature megakaryocytes retained in the constrained ECM microenvironment of the bone marrow, associated with an upregulation of activated β1 integrin in treated mice. Interestingly, previous research by K. Hoffmeister's group has demonstrated that proper megakaryocyte localization at the sinusoids depends on β1 integrin glycosylation. Specifically, the absence of galactosylation in β4galt1$^{-/-}$ megakaryocytes leads to hyperactivity of β1 integrin, which negatively impacts the formation of the DMS (Giannini et al., 2020). Building on these insights, our study shows the coordinated interplay between integrin-mediated signaling and MMP proteolysis, working together to tightly regulate the density and cross-linking properties of the ECM cage and thereby control megakaryocyte maturation at the bone marrow-blood interface. Intriguingly, despite these effects on megakaryocyte maturation, we observed no significant changes in circulating platelet counts, and importantly, platelet function remained preserved. This supports the idea that differences in ECM composition can influence the signaling environment and megakaryocyte maturation, but do not fully abrogate platelet function.

437 The influence of ECM features - like fiber length and pore size - on megakaryocyte
438 biology is complex and not yet fully understood. Longer ECM fibers may help cells adhere
439 better (Barriga et al., 2018; Dolega et al., 2021). Larger pores could make it easier for
440 megakaryocytes to mature and to extend proplatelets at the bone marrow-blood interface.
441 Also, the mechanical properties of the ECM, particularly its stiffness, have emerged as critical
442 environmental determinants of megakaryocyte development and function (Abbonante et al.,
443 2017; Aguilar et al., 2016; Guinard et al., 2023; Leiva et al., 2018). Notably, megakaryocytes
444 possess mechanosensing capabilities, primarily mediated by the β3 integrin subunit,
445 enabling them to detect and respond to changes in substrate stiffness (Guinard et al., 2023).
446 The assembly of extracellular matrix (ECM) fibronectin around megakaryopoiesis involves a
447 more complex interplay of integrins, with both β1 and β3 integrins playing essential roles in
448 fibrillogenesis (Abbonante et al., 2024; Guinard et al., 2023). This cooperative relationship
449 appears to be conserved across various cell types (Attieh et al., 2017; De Mets et al., 2019;
450 Kyumurkov et al., 2023). This may explain why the deletion of both integrins is required to
451 affect the 3D ECM cage and megakaryocyte behavior significantly. We can not exclude that
452 other ECM ligands of β3 integrins, such as fibronectin, may contribute to the organization of
453 collagen IV and laminin, influencing the overall architecture of the vascular niche (Petito &
454 Gresele, 2024; Yang et al., 2022; Zeng et al., 2018). Indeed, it is known that the fibronectin
455 matrix favors the deposition of other ECM proteins, such as collagens IV and various other
456 glycoproteins (Saunders & Schwarzbauer, 2019). This hypothesis underscores the need for
457 further investigation into the spatio-temporal dynamics of ECM component assembly in the
458 megakaryocyte vascular niche.
459 Overall, our findings reveal the supportive role of the ECM cage in platelet
460 biogenesis. Integrin-mediated ECM interactions are clearly crucial, as demonstrated by the
461 50% reduction in platelet counts observed in integrin double knockout mice. In summary,
462 the ECM cage acts as a finely tuned facilitator, optimising the efficiency and precision of
463 platelet production by guiding megakaryocytes to the right place at the right time.
464

465

466 ## MATERIAL and METHODS

467 *Animals.* We used wild type (WT) mice (C57BL/6J from C. River, L'Arbesle, France), Itgb1$^{-/-}$
468 /Itgb3$^{-/-}$ double knock out mice and Pf4cre mice aged 10 to 15 weeks. Pf4cre mice expressed
469 the Cre recombinase under the control of the Pf4 promoter. The β1$^{fl/fl}$ (Potocnik et al.,
470 2000) and β3$^{fl/fl}$ (Morgan et al., 2010) mice were crossed with mice expressing the Cre
471 recombinase under the control of the Pf4 promoter to obtain inactivation in the MK lineage.
472 *Itgb1$^{-/-}$/Itgb3$^{-/-}$* double knock out (KO) mice were crosses of the two single KO lines, as
473 described in Guinard et al., 2023. *GPVI $^{-/-}$* mice and *Lamα4$^{-/-}$* mice were from Nieswandt and
474 Qian labs (Bender et al., 2011; Cai et al., 2022). All animal studies were approved by the
475 French legislation for animal experimentation and in accordance with the guide for the care
476 and use of laboratory animals as defined by the European laws (Animal Facility Agreement C-
477 67-482-10).

478

479 *Chemicals.* Dimethyl sulfoxide (2438), bovine serum albumin (900.011), saponin (47036),
480 Triton X-100 (T8787), fibrinogen and batimastat (SML0041) (Sigma-Aldrich, Rueil-Malmaison,
481 France), Ilomastat (GM6001, HY-15768) (MedChemExpress, Clinisciences, France),
482 Dulbecco's modified Eagle's medium (DMEM), penicillin, streptomycin, and glutamine
483 (Invitrogen , Cergy-Pontoise, France), Gelatin-Oregon Green 488 conjugate (G-13186) (Life
484 Technologies), Laminin 511 recombinant (Biolamina) and fibronectin from human plasma
485 from (341635, Calbiochem) were used in this study.

486

487 *Antibodies.* See Tables 1 and 2 in "Data Supplements" for details.
488 GPIX and GPIbβ are components of the GPIb-IX complex, identifying mature megakaryocytes
489 (Lepage et al., 2000). The choice of marker used to identify megakaryocytes in different
490 experiments is primarily based on technical considerations. Intravital experiments have been
491 standardised using AF488-conjugated anti-GPIX to consistently identify mature
492 megakaryocytes. The rest of the manuscript uses GPIbβ (GP1bβ) due to its strong, specific,
493 bright staining.

494 *Extrusion and Preservation of Murine Bone Marrow.* Bone marrow extrusion, without leaving
495 any residual bone, was obtained by carefully flushing the femurs of mice with PBS using a 21-

496 gauge needle attached to a 10 mL syringe (see photo in Figure 1D) (Scandola et al., 2021). To
497 maximize the preservation of the bone marrow integrity, we used a double fixation
498 procedure (4 % paraformaldehyde and 0.4% glutaraldehyde for 1 hour) immediately after
499 bone marrow extrusion, followed by embedding it in 4 % low-melting-point agarose to
500 preserve as much as possible their three-dimensional architecture.

501 *Isolation of freshly isolated bone marrow-derived megakaryocytes.* Bone marrow
502 megakaryocytes were dissociated using a 21G needle and filtered through a 40 µm Millipore
503 filter. The filter was then rinsed in DMEM + 1% fœtal bovine serum, and the isolated
504 megakaryocytes were adjusted to 300 cells/ml in the same medium.

505 *2D confocal microscopy on bone marrow cryosections.* This study explores the interactions
506 between megakaryocytes and their immediate ECM microenvironment. Ultrathin
507 cryosections were used for their superior axial resolution, offering a 2- to 3-fold
508 improvement over conventional confocal microscopy, which facilitates analysis of signal
509 superposition. Cryosections from WT extruded bone marrow were used to study the ECM
510 composition and distribution of sinusoid-associated megakaryocytes. Bone marrow was
511 fixed in a mix of 2 % paraformaldehyde-0.2 % glutaraldehyde in 0.2 M sodium cacodylate
512 buffer for 1 hour. The fixed samples were infiltrated with 2.3 M sucrose and frozen in liquid
513 nitrogen. Ultrathin cryosections of 250 nm were obtained at −110°C with a LEICA Ultracut
514 UCT cryo-ultramicrotome (Leica Microsystems). For immunofluorescence staining,
515 cryosections were labeled with primary antibodies and conjugated-second antibodies of the
516 appropriate species and DAPI, as reported in Table 1. They were examined under a confocal
517 microscope (TCS SP8, Leica) using the 63x objective with a numerical zoom of 4 (pixel size:
518 0.09µm). The bone marrow specimens from 3 mice were examined under identical
519 conditions, using constant exposure and the same irrelevant antibodies. No fluorescence
520 was detected using isotype-specific control IgG.

521 *3D confocal analysis on bone marrow vibratome sections.* Whole-mount bone marrow
522 preparations were used to investigate i) the localization of megakaryocytes in the bone
523 marrow and the lung and ii) the spatial organization of ECM around sinusoid-associated
524 megakaryocytes. Megakaryocytes were classified based on their maturation stage: stage I
525 (presence of granules, no clear DMS visible), stage II (developing DMS not yet organized),

526 and stage III (DMS organized in platelet territories). Mice from each genotype were analyzed
527 and image acquisitions were performed in a blinded manner.

528 For megakaryocyte localization, sections of femurs's bone marrow or lungs fixed in 2%
529 paraformaldehyde and 0.2% glutaraldehyde for 1 hour, with a thickness of 250 µm, were
530 incubated with FABP4 overnight. This was followed by overnight staining with Alexa 568-
531 conjugated anti-GPIbβ antibody and Alexa 488 Donkey anti-Goat for FABP4. Finally, Hoechst
532 33342 was used for counterstaining for 10 minutes. The fluorescently labeled tissue was
533 placed cut-face down into incubation chambers and mounted with Mowiol mounting
534 solution. The Leica SP8 confocal microscope was used to collect a series of x-y-z images. The
535 images were typically 194x194 µm x-y size and were collected along the z-axis at 1 µm step
536 size through 50 µm of bone marrow tissue. The 40x objective with a numerical zoom of 4
537 (pixel size: 0.142 µm) was used. The lung was imaged using an x63 objective with a 2.5
538 digital zoom (pixel size: 0.145 µm).

539 To perform 3D ECM analysis, bone marrow samples were fixed in 4% PFA and 0.4% GA for 1
540 hour, then embedded in 4% agarose and cut into 250 µm-thick sections using a vibratome.
541 These sections were then incubated overnight at 4°C with primary antibodies targeting
542 laminin, type IV collagen, fibronectin, and fibrinogen, followed by corresponding secondary
543 antibodies and Hoechst 33342 counterstaining. Series of x-y-z images of typically
544 46.13*46.13 µm x-y size were collected along the z-axis at 1 µm step size through 15-35 µm
545 of sinusoid-associated megakaryocytes, using the 63x objective with a numerical zoom of 4
546 (pixel size: 0.09) from a Leica SP8 confocal microscope. For quantitative spatial analysis of
547 ECM around megakaryocytes, the observations have been made on z-stacks as described by
548 *Voisin et al.* (Voisin et al., 2010).The fluorescence was delineated on the maximum z-stack
549 projection of half a megakaryocyte using Image J software.

550 Image processing to perform quantitative analyses of fluorescence profiles and fiber length
551 are explained in Suppl. Figure 7. The random length measurement method uses random
552 sampling to provide unbiased data on laminin/collagen fibers in a 3D cage. Measurements
553 included intervals between different branching points throughout the cage, including branch
554 ends. Processing involved five steps: 1) acquiring 3D images, 2) projecting onto 2D planar
555 sections, 3) selecting random intersection points for measurement, 4) measuring intervals
556 using ImageJ software, and 5) repeating the process for a representative dataset. Briefly, a

557 binary threshold mask (0 for the background and 1 for the ECM network, threshold to
558 reduce signal noise) was generated from the channel showing labeled collagen or laminin.
559 The mask was then applied to the channel showing megakaryocytes, resulting in an image
560 that corresponded to only an active ECM signal that colocalized with megakaryocytes. The
561 mask was then applied to the collagen/laminin channel to determine the amount of
562 fluorescent ECM within the mask. This enabled the determination of the cell area and the
563 elimination of the signal outside the mask.
564
565 *Intravital imaging.* *Pf4cre* and *Itgb1*$^{-/-}$/*Itgb3*$^{-/-}$ mice underwent intravital imaging. To visualize
566 megakaryocytes and sinusoids, an AF488-conjugated anti-GPIX antibody derivative and
567 Texas Red dextran 70kDa were intravenously injected, respectively. The skull bone marrow
568 was observed using two-photon microscopy, following the procedure described in reference
569 (Bornert et al., 2021). The anesthetized mice were monitored for a maximum of 6 hours,
570 during which one to four proplatelets were recorded. Two regions of interest were analyzed,
571 each composed of 3 images (xyz = 1320 µm*1320 µm*100 µm, total volume/ROI = 0.17
572 µm3, pixel size = 0.867 µm at obj HC FLUOTAR L 25x/0.95 WATER zoom x1). A total of 130
573 megakaryocytes *PF4cre* vs. 130 megakaryocytes *Itgb1*$^{-/-}$/*Itgb3*$^{-/-}$ were analyzed and the
574 results are expressed in %.
575
576 *Electron microscopy.* For Transmission electron microscopy, bone marrow was fixed in 2.5%
577 glutaraldehyde for 1 hour and embedded in Epon as described (Scandola et al., 2021).
578 Transversal thin sections of the entire bone marrow were cut and examined under a JEOL
579 TEM (120 kV). The number of megakaryocytes was counted per surface unit (s.u., 12,945
580 µm2). The observations from three independent mice were averaged.
581 For SEM, native bone marrow megakaryocytes were allowed to adhere to a surface coated
582 with 300 µg/ml fibronectin, 100 µg/ml fibrinogen, or 50 µg/ml laminin 511. After gentle
583 agitation to detach non-adherent cells, the remaining adherent cells were fixed in 2.5 %
584 glutaraldehyde for 1 hour, dehydrated, attached to stubs, sputter coated, and examined
585 under a Helios NanoLab microscope at 5kV (ThermoFisher, Eindhoven, The Netherlands).
586 Adherent megakaryocytes where counted and classified as spreading or round cells. The
587 results were obtained by the average from three independent mice.
588

589 *Flow cytometry.* Flow cytometry was used to investigate i) megakaryocyte ploidy, ii) intact
590 megakaryocytes in the blood and iii) platelet activation.
591 For the ploidy analysis of the native megakaryocytes, mouse femurs, tibias, and iliac crests
592 were harvested, cut into small fragments, and incubated in a PBS-collagenase-dispase mix
593 (at 3 mg/mL and 4 mg/mL, 5mL/mouse respectively) for 30 min at 37°C. Then, the tube was
594 filled with PBS-2% NCS to stop the collagenase, and the supernatant was 70 µm filtered to
595 eliminate the bone fragments. After red cell lysis, the freshly isolated bone marrows were
596 washed in PBS-2% NCS and stained with anti-CD41 and anti-CD42c antibodies and Hoechst.
597 Anti Gr-1, B220, F4/80, and TER119 probes were used as a negative control to exclude
598 granulocytes, B lymphocytes, macrophages, and erythrocytes from the total bone marrow
599 suspension. The freshly isolated megakaryocytes were identified as a CD41/CD42c positive
600 cell population and ploidy analysis was performed using Hoechst 33342. The results are
601 representative of three independent experiments.
602 For detection of intact megakaryocytes in the blood, red blood cell lysis was performed using
603 BD Lysing buffer solution according to manufacturer's instruction. The resulting
604 mononucleated cells were labelled with fluorescent conjugated antibodies: anti CD41-PE-
605 Cy7 (clone MWReg30), anti-CD42c-Alexa 488 (clone RAM-1), anti-CD45-PE (clone 30-F11),
606 TER119-APC (clone TER119), antibodies from ebiosciences except RAM-1 antibody produced
607 in house. Megakaryocytes enriched from bone marrow using BSA gradient were spiked into
608 blood sample to validate the gating strategy to identify potential circulating megakaryocytes
609 as $CD45^{+}TER119^{-}CD41^{+}CD42c^{+}$ events. 300.10^{3} $CD45^{+}TER119^{-}$ events were recorded. Data
610 acquisition was performed on a Symphony A1 flow cytometer (BD Biosciences) and analyzed
611 using BD FACS Diva Software (BD Biosciences).

612 For platelet activation studies, whole blood was collected from the tail vein and
613 anticoagulated with hirudin (200 U /ml). Platelets were activated or not with collagen-
614 related peptide (CRP, 40 µg/ml) and TRAP (4mM) for 15 min at 37°C and stained with FITC-
615 labelled or 647-labelled rat anti-mouse GPIbβ and APC-labeled rat anti-mouse P-selectin or
616 PE-labelled rat anti-mouse activated-αIIbβ3 antibodies. Fluorescence was quantified using
617 an LSRFortessa cell analyze (BD Biosciences) and BD FACSDiva software. A total of 20.000
618 events were analyzed for each sample.

619

620 *Microfluidic experiments.* The PDMS microfluidic chamber channels were assembled and
621 connected to a peristaltic pump, as described (Osmani et al., 2021). The channels were
622 washed with PBS for 5 min and coated with laminin 511 (50 µg/ml), fibrillar fibronectin (300
623 µg/ml), or fibrinogen (100 µg/ml) overnight at 4°C, followed by a blocking stage with human
624 serum albumin (1 %) for 30 min at RT. To produce fibrillar fibronectin, we use the method of
625 mechanical stretching as described in Maurer et al, (Maurer et al., 2015). Freshly isolated
626 megakaryocytes were seeded at a concentration of 30 cells /µL per channel and incubated
627 for 15 min – 45 min at 37 °C with 5 % CO_2. In previous work, the seeding time was
628 determined with capture efficiencies of over 80 % for Pf4cre megakaryocytes (Suppl. Figure
629 4B). The channels were then perfused under a flow of 300 µm/s and the megakaryocyte
630 behavior was monitored in real-time, for 1 min, using a Leica DMI8 microscope (x20)
631 equipped with a CMOS Camera (Hamamatsu ORCA fusion). Megakaryocyte capture yield was
632 measured by quantifying the number of adherent megakaryocytes before and after flow
633 induction (expressed as a percentage) on an average of 20 stage positions (n= 50
634 megakaryocytes analyzed/test). The results are an average of three independent
635 experiments, the values were expressed as a mean ± sem.
636
637 *Bone marrow explants.* Preparation of bone marrow explants was performed as described in
638 Guinard et al., 2021 to investigate proplatelet formation. For investigating megakaryocyte
639 emigration, bone marrows were flushed from femurs of *Pf4cre* and*Itgb1*$^{-/-}$/*Itgb3*$^{-/-}$; Lamα4$^{+/+}$
640 and Lamα4$^{-/-}$; as well as from DMSO- and B+I-treated mice and ten 0.5 mm-thick sections
641 were placed in an incubation chamber. Megakaryocytes at the periphery of the explants
642 were counted under an inverted phase contrast microscope coupled to a video camera
643 (DMI8 Leica microscope, 40x objective). A motorized multiposition stage (in *x, y*, *z*) was used,
644 and an average of 100 stages positions showing megakaryocytes was followed. Results are
645 expressed as the number of total emigrating megakaryocytes at the indicated time points. In
646 each case, a minimum of six independent experiments were performed. Mice from each
647 genotype were analyzed and image acquisitions were performed in a blinded manner.
648
649 *Effects of MMP inhibition.* Batimastat plus ilomastat treatment was tested for their potential
650 impact on the ECM in the microenvironment of the megakaryocyte vascular niche. Mice
651 were treated daily with a protease inhibitor cocktail (Batimastat at 30 mg/kg + Ilomastat at

652 50 mg/kg) or vehicle (DMSO) for 7 consecutive days (Gui et al., 2018; Pielecka-Fortuna et al.,
653 2015). The platelet count was monitored every two days. On the eighth day, the mice were
654 sacrificed, and their bone marrow was collected for analysis of ECM organization and
655 megakaryocyte behavior, as explained in the 3D confocal analysis on bone marrow
656 vibratome sections.

657 *Gelatin degradation assay.* Coverslips were coated with Oregon green gelatin, and fixed with
658 0.5% glutaraldehyde for 20 min at RT. After washing three times with PBS, cells were seeded
659 on coated coverslips and incubated for 6 h before fixation and staining.

660 *Statistics.* All values are reported as the mean ± sem. n= number of megakaryocytes studied.
661 Statistical analyses were performed with PrismGraphpad software (La Jolla, CA, USA). For
662 group comparison, data were tested for Gaussian distribution. Then, a Student t-test
663 (Gaussian) or Mann-Whitney U test (non-Gaussian) were used to compare individual groups;
664 multiple groups were compared by one-way ANOVA followed by Bonferroni post-test or by a
665 non-parametric Kruskal-Wallis test, with a threshold of significance of 5%. P-values <0.05
666 were considered statistically significant. *P<0.05; **P<0.01; ***P<0.001.
667

Contributions

C.M and C.S performed experiments, analyzed data, and contributed to the writing of the revised manuscript; JY.R, F.P, E.J-B, N.O, L.M, A.M., N.B. and A.B performed experiments, analyzed data, and commented on the manuscript; J.G, N.O, C.Q, F.B, and C.L provided vital reagents and commented on the manucript; R.P., O.D, and M.L contributed to the writing of the manuscript; and A.E designed and supervised research, analyzed data, and wrote the manuscript

Acknowledgments

We wish to thank Ketty Knez-Hippert, Josiane Weber, Clarisse Mouriaux, Sylvie Moog and Patricia Laeuffer (EFS-GEST) for excellent expert technical assistance. This work was supported by ARMESA (Association de Recherche et Développement en Médecine et Santé Publique) and by ANR Grant MegaPod (ANR-22-CE14-0029). The authors thank Pr. B. Nieswandt for providing GPVI knock-out mice.

Discosure of conflicts of interest

The authors have no conflicts of interests to declare

688 ## References

689

690 Abbonante, V., Chitalia, V., Rosti, V., Leiva, O., Matsuura, S., Balduini, A., & Ravid, K. (2017).
691 Upregulation of lysyl oxidase and adhesion to collagen of human megakaryocytes and
692 platelets in primary myelofibrosis. *Blood*, *130*(6), 829-831. https://doi.org/10.1182/blood-
693 2017-04-777417

694 Abbonante, V., Di Buduo, C. A., Gruppi, C., Malara, A., Gianelli, U., Celesti, G., Anselmo, A., Laghi, L.,
695 Vercellino, M., Visai, L., Iurlo, A., Moratti, R., Barosi, G., Rosti, V., & Balduini, A. (2016).
696 Thrombopoietin/TGF- *β* 1 Loop Regulates Megakaryocyte Extracellular Matrix Component
697 Synthesis. *Stem Cells*, *34*(4), 1123-1133. https://doi.org/10.1002/stem.2285

698 Abbonante, V., Karkempetzaki, A. I., Leon, C., Krishnan, A., Huang, N., Di Buduo, C. A., Cattaneo, D.,
699 Ward, C. M., Matsuura, S., Guinard, I., Weber, J., De Acutis, A., Vozzi, G., Iurlo, A., Ravid, K., &
700 Balduini, A. (2024). Newly identified roles for PIEZO1 mechanosensor in controlling normal
701 megakaryocyte development and in primary myelofibrosis. *American Journal of Hematology*,
702 *99*(3), 336-349. https://doi.org/10.1002/ajh.27184

703 Aguilar, A., Pertuy, F., Eckly, A., Strassel, C., Collin, D., Gachet, C., Lanza, F., & Léon, C. (2016).
704 Importance of environmental stiffness for megakaryocyte differentiation and proplatelet
705 formation. *Blood*, *128*(16), 2022-2032. https://doi.org/10.1182/blood-2016-02-699959

706 Attieh, Y., Clark, A. G., Grass, C., Richon, S., Pocard, M., Mariani, P., Elkhatib, N., Betz, T., Gurchenkov,
707 B., & Vignjevic, D. M. (2017). Cancer-associated fibroblasts lead tumor invasion through
708 integrin-β3–dependent fibronectin assembly. *Journal of Cell Biology*, *216*(11), 3509-3520.
709 https://doi.org/10.1083/jcb.201702033

710 Avecilla, S. T., Hattori, K., Heissig, B., Tejada, R., Liao, F., Shido, K., Jin, D. K., Dias, S., Zhang, F.,
711 Hartman, T. E., Hackett, N. R., Crystal, R. G., Witte, L., Hicklin, D. J., Bohlen, P., Eaton, D.,
712 Lyden, D., De Sauvage, F., & Rafii, S. (2004). Chemokine-mediated interaction of
713 hematopoietic progenitors with the bone marrow vascular niche is required for
714 thrombopoiesis. *Nature Medicine*, *10*(1), 64-71. https://doi.org/10.1038/nm973

715 Balduini, A., Pallotta, I., Malara, A., Lova, P., Pecci, A., Viarengo, G., Balduini, C. L., & Torti, M. (2008).
716 Adhesive receptors, extracellular proteins and myosin IIA orchestrate proplatelet formation
717 by human megakaryocytes. *Journal of Thrombosis and Haemostasis: JTH*, *6*(11), 1900-1907.
718 https://doi.org/10.1111/j.1538-7836.2008.03132.x

719 Barriga, E. H., Franze, K., Charras, G., & Mayor, R. (2018). Tissue stiffening coordinates
720 morphogenesis by triggering collective cell migration in vivo. *Nature*, *554*(7693), 523-527.
721 https://doi.org/10.1038/nature25742

722 Bender, M., Hagedorn, I., & Nieswandt, B. (2011). Genetic and antibody-induced glycoprotein VI
723 deficiency equally protects mice from mechanically and FeCl3-induced thrombosis. *Journal of*
724 *Thrombosis and Haemostasis*, *9*(7), 1423-1426. https://doi.org/10.1111/j.1538-
725 7836.2011.04328.x

726 Bornert, A., Boscher, J., Pertuy, F., Eckly, A., Stegner, D., Strassel, C., Gachet, C., Lanza, F., & Léon, C.
727 (2021). Cytoskeletal-based mechanisms differently regulate *in vivo* and *in vitro* proplatelet
728 formation. *Haematologica*, *106*(5), Article 5. https://doi.org/10.3324/haematol.2019.239111

729 Boscher, J., Guinard, I., Eckly, A., Lanza, F., & Léon, C. (2020). Blood platelet formation at a glance.
730 *Journal of Cell Science*, *133*(20), jcs244731. https://doi.org/10.1242/jcs.244731

731 Cai, H., Kondo, M., Sandhow, L., Xiao, P., Johansson, A.-S., Sasaki, T., Zawacka-Pankau, J., Tryggvason,
732 K., Ungerstedt, J., Walfridsson, J., Ekblom, M., & Qian, H. (2022). Critical role of Lama4 for
733 hematopoiesis regeneration and acute myeloid leukemia progression. *Blood*, *139*(20),
734 3040-3057. https://doi.org/10.1182/blood.2021011510
735 De Mets, R., Wang, I., Balland, M., Oddou, C., Moreau, P., Fourcade, B., Albiges-Rizo, C., Delon, A., &
736 Destaing, O. (2019). Cellular tension encodes local Src-dependent differential β_1 and β_3
737 integrin mobility. *Molecular Biology of the Cell*, *30*(2), 181-190.
738 https://doi.org/10.1091/mbc.E18-04-0253
739 Dolega, M. E., Monnier, S., Brunel, B., Joanny, J.-F., Recho, P., & Cappello, G. (2021). Extracellular
740 matrix in multicellular aggregates acts as a pressure sensor controlling cell proliferation and
741 motility. *eLife*, *10*, e63258. https://doi.org/10.7554/eLife.63258
742 Eliades, A., Papadantonakis, N., Bhupatiraju, A., Burridge, K. A., Johnston-Cox, H. A., Migliaccio, A. R.,
743 Crispino, J. D., Lucero, H. A., Trackman, P. C., & Ravid, K. (2011). Control of Megakaryocyte
744 Expansion and Bone Marrow Fibrosis by Lysyl Oxidase. *Journal of Biological Chemistry*,
745 *286*(31), 27630-27638. https://doi.org/10.1074/jbc.M111.243113
746 Frydman, G. H., Ellett, F., Jorgensen, J., Marand, A. L., Zukerberg, L., Selig, M. K., Tessier, S. N., Wong,
747 K. H. K., Olaleye, D., Vanderburg, C. R., Fox, J. G., Tompkins, R. G., & Irimia, D. (2023).
748 Megakaryocytes respond during sepsis and display innate immune cell behaviors. *Frontiers in*
749 *Immunology*, *14*, 1083339. https://doi.org/10.3389/fimmu.2023.1083339
750 Gaertner, F., Ishikawa-Ankerhold, H., Stutte, S., Fu, W., Weitz, J., Dueck, A., Nelakuditi, B., Fumagalli,
751 V., Van Den Heuvel, D., Belz, L., Sobirova, G., Zhang, Z., Titova, A., Navarro, A. M., Pekayvaz,
752 K., Lorenz, M., Von Baumgarten, L., Kranich, J., Straub, T., … Massberg, S. (2024).
753 Plasmacytoid dendritic cells control homeostasis of megakaryopoiesis. *Nature*, *631*(8021),
754 645-653. https://doi.org/10.1038/s41586-024-07671-y
755 Gelon, L., Fromont, L., & Lefrançais, E. (2022). Occurrence and role of lung megakaryocytes in
756 infection and inflammation. *Frontiers in Immunology*, *13*.
757 https://www.frontiersin.org/articles/10.3389/fimmu.2022.1029223
758 Gianelli, U., Thiele, J., Orazi, A., Gangat, N., Vannucchi, A. M., Tefferi, A., & Kvasnicka, H. M. (2023).
759 International Consensus Classification of myeloid and lymphoid neoplasms : 760 Myeloproliferative neoplasms. *Virchows Archiv*, *482*(1), 53-68.
761 https://doi.org/10.1007/s00428-022-03480-8
762 Giannini, S., Lee-Sundlov, M. M., Rivadeneyra, L., Di Buduo, C. A., Burns, R., Lau, J. T., Falet, H.,
763 Balduini, A., & Hoffmeister, K. M. (2020). β4GALT1 controls β1 integrin function to govern
764 thrombopoiesis and hematopoietic stem cell homeostasis. *Nature Communications*, *11*(1),
765 356. https://doi.org/10.1038/s41467-019-14178-y
766 Gui, P., Ben-Neji, M., Belozertseva, E., Dalenc, F., Franchet, C., Gilhodes, J., Labrousse, A., Bellard, E.,
767 Golzio, M., Poincloux, R., Maridonneau-Parini, I., & Le Cabec, V. (2018). The Protease-
768 Dependent Mesenchymal Migration of Tumor-Associated Macrophages as a Target in Cancer
769 Immunotherapy. *Cancer Immunology Research*, *6*(11), 1337-1351.
770 https://doi.org/10.1158/2326-6066.CIR-17-0746
771 Guinard, I., Nguyen, T., Brassard-Jollive, N., Weber, J., Ruch, L., Reininger, L., Brouard, N., Eckly, A.,
772 Collin, D., Lanza, F., & Léon, C. (2023). Matrix stiffness controls megakaryocyte adhesion,
773 fibronectin fibrillogenesis, and proplatelet formation through Itgβ3. *Blood Advances*, *7*(15),
774 4003-4018. https://doi.org/10.1182/bloodadvances.2022008680

775 Hamada, T., Möhle, R., Hesselgesser, J., Hoxie, J., Nachman, R. L., Moore, M. A. S., & Rafii, S. (1998).
776 Transendothelial Migration of Megakaryocytes in Response to Stromal Cell-derived Factor 1
777 (SDF-1) Enhances Platelet Formation. *Journal of Experimental Medicine*, *188*(3), 539-548.
778 https://doi.org/10.1084/jem.188.3.539
779 Handagama, P. J., George, J. N., Shuman, M. A., McEver, R. P., & Bainton, D. F. (1987). Incorporation
780 of a circulating protein into megakaryocyte and platelet granules. *Proceedings of the*
781 *National Academy of Sciences*, *84*(3), 861-865. https://doi.org/10.1073/pnas.84.3.861
782 Janus-Bell, E., Receveur, N., Mercier, L., Mouriaux, C., Magnenat, S., Reiser, J., Lanza, F., Hechler, B.,
783 Ho-Tin-Noé, B., & Mangin, P. H. (2024). Cooperation Between Platelet β1 and β3 Integrins in
784 the Arrest of Bleeding Under Inflammatory Conditions in Mice—Brief Report. *Arteriosclerosis,*
785 *Thrombosis, & Vascular Biology*, *44*(10), 2213-2222.
786 https://doi.org/10.1161/ATVBAHA.124.321104
787 Kyumurkov, A., Bouin, A.-P., Boissan, M., Manet, S., Baschieri, F., Proponnet-Guerault, M., Balland,
788 M., Destaing, O., Régent-Kloeckner, M., Calmel, C., Nicolas, A., Waharte, F., Chavrier, P.,
789 Montagnac, G., Planus, E., & Albiges-Rizo, C. (2023). Force tuning through regulation of
790 clathrin-dependent integrin endocytosis. *Journal of Cell Biology*, *222*(1), e202004025.
791 https://doi.org/10.1083/jcb.202004025
792 Larsen, M., Artym, V. V., Green, J. A., & Yamada, K. M. (2006). The matrix reorganized : Extracellular
793 matrix remodeling and integrin signaling. *Current Opinion in Cell Biology*, *18*(5), 463-471.
794 https://doi.org/10.1016/j.ceb.2006.08.009
795 Larson, M. K., & Watson, S. P. (2006). Regulation of proplatelet formation and platelet release by
796 integrin αIIbβ3. *Blood*, *108*(5), 1509-1514. https://doi.org/10.1182/blood-2005-11-011957
797 Leiva, O., Leon, C., Ng, S. K., Mangin, P., Gachet, C., & Ravid, K. (2018). The Role of Extracellular
798 Matrix Stiffness in Megakaryocyte Development and Function. *American journal of*
799 *hematology*, *93*(3), 430-441. https://doi.org/10.1002/ajh.25008
800 Lemmon, C. A., Chen, C. S., & Romer, L. H. (2009). Cell Traction Forces Direct Fibronectin Matrix
801 Assembly. *Biophysical Journal*, *96*(2), 729-738. https://doi.org/10.1016/j.bpj.2008.10.009
802 Lepage, A., Leboeuf, M., Cazenave, J. P., de la Salle, C., Lanza, F., & Uzan, G. (2000). The
803 alpha(IIb)beta(3) integrin and GPIb-V-IX complex identify distinct stages in the maturation of
804 CD34(+) cord blood cells to megakaryocytes. *Blood*, *96*(13), 4169-4177.
805 Lichtman, M. A., Chamberlain, J. K., Simon, W., & Santillo, P. A. (1978). Parasinusoidal location of
806 megakaryocytes in marrow : A determinant of platelet release. *American Journal of*
807 *Hematology*, *4*(4), 303-312. https://doi.org/10.1002/ajh.2830040402
808 Malara, A., Currao, M., Gruppi, C., Celesti, G., Viarengo, G., Buracchi, C., Laghi, L., Kaplan, D. L., &
809 Balduini, A. (2014). Megakaryocytes contribute to the bone marrow-matrix environment by
810 expressing fibronectin, type IV collagen and laminin. *Stem cells (Dayton, Ohio)*, *32*(4),
811 926-937. https://doi.org/10.1002/stem.1626
812 Malara, A., Gruppi, C., Abbonante, V., Cattaneo, D., De Marco, L., Massa, M., Iurlo, A., Gianelli, U.,
813 Balduini, C. L., Tira, M. E., Muro, A. F., Chauhan, A. K., Rosti, V., Barosi, G., & Balduini, A.
814 (2019). EDA fibronectin–TLR4 axis sustains megakaryocyte expansion and inflammation in
815 bone marrow fibrosis. *Journal of Experimental Medicine*, *216*(3), 587-604.
816 https://doi.org/10.1084/jem.20181074
817 Malara, A., Ligi, D., Di Buduo, C. A., Mannello, F., & Balduini, A. (2018). Sub-Cellular Localization of
818 Metalloproteinases in Megakaryocytes. *Cells*, *7*(7), Article 7.
819 https://doi.org/10.3390/cells7070080

Matsuura, S., Thompson, C. R., Ng, S. K., Ward, C. M., Karagianni, A., Mazzeo, C., Malara, A., Balduini, A., & Ravid, K. (2020). Adhesion to fibronectin via α5β1 integrin supports expansion of the megakaryocyte lineage in primary myelofibrosis. *Blood*, *135*(25), 2286-2291. https://doi.org/10.1182/blood.2019004230

Maurer, E., Schaff, M., Receveur, N., Bourdon, C., Mercier, L., Nieswandt, B., Dubois, C., Jandrot-Perrus, M., Goetz, J. G., Lanza, F., Gachet, C., & Mangin, P. H. (2015). Fibrillar cellular fibronectin supports efficient platelet aggregation and procoagulant activity. *Thrombosis and Haemostasis*, *114*(12), 1175-1188. https://doi.org/10.1160/TH14-11-0958

Morgan, E. A., Schneider, J. G., Baroni, T. E., Uluçkan, O., Heller, E., Hurchla, M. A., Deng, H., Floyd, D., Berdy, A., Prior, J. L., Piwnica-Worms, D., L. Teitelbaum, S., Patrick Ross, F., & Weilbaecher, K. N. (2010). Dissection of platelet and myeloid cell defects by conditional targeting of the β3-integrin subunit. *The FASEB Journal*, *24*(4), 1117-1127. https://doi.org/10.1096/fj.09-138420

Oprescu, A., Michel, D., Antkowiak, A., Vega, E., Viaud, J., Courtneidge, S. A., Eckly, A., De La Salle, H., Chicanne, G., Léon, C., Payrastre, B., & Gaits-Iacovoni, F. (2022). Megakaryocytes form linear podosomes devoid of digestive properties to remodel medullar matrix. *Scientific Reports*, *12*(1), 6255. https://doi.org/10.1038/s41598-022-10215-x

Osmani, N., Follain, G., Gensbittel, V., García-León, M. J., Harlepp, S., & Goetz, J. G. (2021). Probing Intravascular Adhesion and Extravasation of Tumor Cells with Microfluidics. In U. S. Stein (Éd.), *Metastasis* (Vol. 2294, p. 111-132). Springer US. https://doi.org/10.1007/978-1-0716-1350-4_8

Ouzegdouh, Y., Capron, C., Bauer, T., Puymirat, E., Diehl, J.-L., Martin, J. F., & Cramer-Bordé, E. (2018). The physical and cellular conditions of the human pulmonary circulation enable thrombopoiesis. *Experimental Hematology*, *63*, 22-27.e3. https://doi.org/10.1016/j.exphem.2018.04.001

Petito, E., & Gresele, P. (2024). Immune attack on megakaryocytes in immune thrombocytopenia. *Research and Practice in Thrombosis and Haemostasis*, *8*(1), 102345. https://doi.org/10.1016/j.rpth.2024.102345

Petrey, A. C., Obery, D. R., Kessler, S. P., Flamion, B., & De La Motte, C. A. (2016). Hyaluronan Depolymerization by Megakaryocyte Hyaluronidase-2 Is Required for Thrombopoiesis. *The American Journal of Pathology*, *186*(9), 2390-2403. https://doi.org/10.1016/j.ajpath.2016.05.004

Pielecka-Fortuna, J., Kalogeraki, E., Fortuna, M. G., & Löwel, S. (2015). Optimal level activity of matrix metalloproteinases is critical for adult visual plasticity in the healthy and stroke-affected brain. *eLife*, *4*, e11290. https://doi.org/10.7554/eLife.11290

Piszczatowski, R. T., Schwenger, E., Sundaravel, S., Stein, C. M., Liu, Y., Stanley, P., Verma, A., Zheng, D., Seidel, R. D., Almo, S. C., Townley, R. A., Bülow, H. E., & Steidl, U. (2022). A glycan-based approach to cell characterization and isolation : Hematopoiesis as a paradigm. *Journal of Experimental Medicine*, *219*(11), e20212552. https://doi.org/10.1084/jem.20212552

Potocnik, A. J., Brakebusch, C., & Fässler, R. (2000). Fetal and Adult Hematopoietic Stem Cells Require β1 Integrin Function for Colonizing Fetal Liver, Spleen, and Bone Marrow. *Immunity*, *12*(6), 653-663. https://doi.org/10.1016/S1074-7613(00)80216-2

Puhm, F., Laroche, A., & Boilard, E. (2023). Diversity of Megakaryocytes. *Arteriosclerosis, Thrombosis, and Vascular Biology*, *43*(11), 2088-2098. https://doi.org/10.1161/ATVBAHA.123.318782

863 Radley, J. M., & Haller, C. J. (1983). Fate of senescent megakaryocytes in the bone marrow. *British*
864 *Journal of Haematology*, *53*(2), 277-287. https://doi.org/10.1111/j.1365-
865 2141.1983.tb02022.x
866 Rapkiewicz, A. V., Mai, X., Carsons, S. E., Pittaluga, S., Kleiner, D. E., Berger, J. S., Thomas, S., Adler, N.
867 M., Charytan, D. M., Gasmi, B., Hochman, J. S., & Reynolds, H. R. (2020). Megakaryocytes and
868 platelet-fibrin thrombi characterize multi-organ thrombosis at autopsy in COVID-19 : A case
869 series. *eClinicalMedicine*, *24*, 100434. https://doi.org/10.1016/j.eclinm.2020.100434
870 Sabri, S., Jandrot-Perrus, M., Bertoglio, J., Farndale, R. W., Mas, V. M.-D., Debili, N., & Vainchenker,
871 W. (2004). Differential regulation of actin stress fiber assembly and proplatelet formation by
872 α2β1 integrin and GPVI in human megakaryocytes. *Blood*, *104*(10), 3117-3125.
873 https://doi.org/10.1182/blood-2003-12-4398
874 Sarachakov, A., Varlamova, A., Svekolkin, V., Polyakova, M., Valencia, I., Unkenholz, C., Pannellini, T.,
875 Galkin, I., Ovcharov, P., Tabakov, D., Postovalova, E., Shin, N., Sethi, I., Bagaev, A., Itkin, T.,
876 Crane, G., Kluk, M., Geyer, J., Inghirami, G., & Patel, S. (2023). Spatial mapping of human
877 hematopoiesis at single-cell resolution reveals aging-associated topographic remodeling.
878 *Blood*, *142*(26), 2282-2295. https://doi.org/10.1182/blood.2023021280
879 Saunders, J. T., & Schwarzbauer, J. E. (2019). Fibronectin matrix as a scaffold for procollagen
880 proteinase binding and collagen processing. *Molecular Biology of the Cell*, *30*(17), 2218-2226.
881 https://doi.org/10.1091/mbc.E19-03-0140
882 Scandola, C., Lanza, F., Gachet, C., & Eckly, A. (2021). In Situ Exploration of Murine Megakaryopoiesis
883 using Transmission Electron Microscopy. *Journal of Visualized Experiments*, *175*, 62494.
884 https://doi.org/10.3791/62494
885 Semeniak, D., Faber, K., Öftering, P., Manukjan, G., & Schulze, H. (2019). Impact of Itga2-Gp6-double
886 collagen receptor deficient mice for bone marrow megakaryocytes and platelets. *PLOS ONE*,
887 *14*(8), e0216839. https://doi.org/10.1371/journal.pone.0216839
888 Semeniak, D., Kulawig, R., Stegner, D., Meyer, I., Schwiebert, S., Bösing, H., Eckes, B., Nieswandt, B.,
889 & Schulze, H. (2016). Proplatelet formation is selectively inhibited by collagen type I through
890 Syk-independent GPVI signaling. *Journal of Cell Science*, *129*(18), 3473-3484.
891 https://doi.org/10.1242/jcs.187971
892 Stegner, D., vanEeuwijk, J. M. M., Angay, O., Gorelashvili, M. G., Semeniak, D., Pinnecker, J.,
893 Schmithausen, P., Meyer, I., Friedrich, M., Dütting, S., Brede, C., Beilhack, A., Schulze, H.,
894 Nieswandt, B., & Heinze, K. G. (2017). Thrombopoiesis is spatially regulated by the bone
895 marrow vasculature. *Nature Communications*, *8*(1), 127. https://doi.org/10.1038/s41467-
896 017-00201-7
897 Stone, A. P., Nascimento, T. F., & Barrachina, M. N. (2022). The bone marrow niche from the inside
898 out : How megakaryocytes are shaped by and shape hematopoiesis. *Blood*, *139*(4), 483-491.
899 https://doi.org/10.1182/blood.2021012827
900 Susek, K. H., Korpos, E., Huppert, J., Wu, C., Savelyeva, I., Rosenbauer, F., Müller-Tidow, C.,
901 Koschmieder, S., & Sorokin, L. (2018). Bone marrow laminins influence hematopoietic stem
902 and progenitor cell cycling and homing to the bone marrow. *Matrix Biology*, *67*, 47-62.
903 https://doi.org/10.1016/j.matbio.2018.01.007
904 Villeneuve, J., Block, A., Le Bousse-Kerdilès, M.-C., Lepreux, S., Nurden, P., Ripoche, J., & Nurden, A. T.
905 (2009). Tissue inhibitors of matrix metalloproteinases in platelets and megakaryocytes : A
906 novel organization for these secreted proteins. *Experimental Hematology*, *37*(7), 849-856.
907 https://doi.org/10.1016/j.exphem.2009.03.009

908 Vögtle, T., Sharma, S., Mori, J., Nagy, Z., Semeniak, D., Scandola, C., Geer, M. J., Smith, C. W., Lane, J.,
909 Pollack, S., Lassila, R., Jouppila, A., Barr, A. J., Ogg, D. J., Howard, T. D., McMiken, H. J.,
910 Warwicker, J., Geh, C., Rowlinson, R., … Senis, Y. A. (2019). Heparan sulfates are critical
911 regulators of the inhibitory megakaryocyte-platelet receptor G6b-B. *eLife*, *8*, e46840.
912 https://doi.org/10.7554/eLife.46840
913 Voisin, M.-B., Pröbstl, D., & Nourshargh, S. (2010). Venular Basement Membranes Ubiquitously
914 Express Matrix Protein Low-Expression Regions : Characterization in Multiple Tissues and
915 Remodeling during Inflammation. *The American Journal of Pathology*, *176*(1), 482-495.
916 https://doi.org/10.2353/ajpath.2010.090510
917 Wang, M., Feng, R., Zhang, J., Xu, L., Feng, F., Wang, C., Wang, Q., Zhu, X., He, Y., Xue, J., Fu, H., Lv,
918 M., Kong, Y., Chang, Y., Xu, L., Liu, K., Huang, X., & Zhang, X. (2019). Dysregulated
919 megakaryocyte distribution associated with nestin+ mesenchymal stem cells in immune
920 thrombocytopenia. *Blood Advances*, *3*(9), 1416-1428.
921 https://doi.org/10.1182/bloodadvances.2018026690
922 Winer, A., Adams, S., & Mignatti, P. (2018). Matrix Metalloproteinase Inhibitors in Cancer Therapy :
923 Turning Past Failures Into Future Successes. *Molecular Cancer Therapeutics*, *17*(6),
924 1147-1155. https://doi.org/10.1158/1535-7163.MCT-17-0646
925 Yang, X., Chitalia, S. V., Matsuura, S., & Ravid, K. (2022). Integrins and their role in megakaryocyte
926 development and function. *Experimental Hematology*, *106*, 31-39.
927 https://doi.org/10.1016/j.exphem.2021.11.007
928 Zeng, D. F., Chen, F., Wang, S., Chen, S. L., Xu, Y., Shen, M. Q., Du, C. H., Wang, C., Kong, P. Y., Cheng,
929 T. M., Su, Y. P., & Wang, J. P. (2018). Autoantibody against integrin αvβ3 contributes to
930 thrombocytopenia by blocking the migration and adhesion of megakaryocytes. *Journal of*
931 *Thrombosis and Haemostasis*, *16*(9), 1843-1856. https://doi.org/10.1111/jth.14214
932

933

934

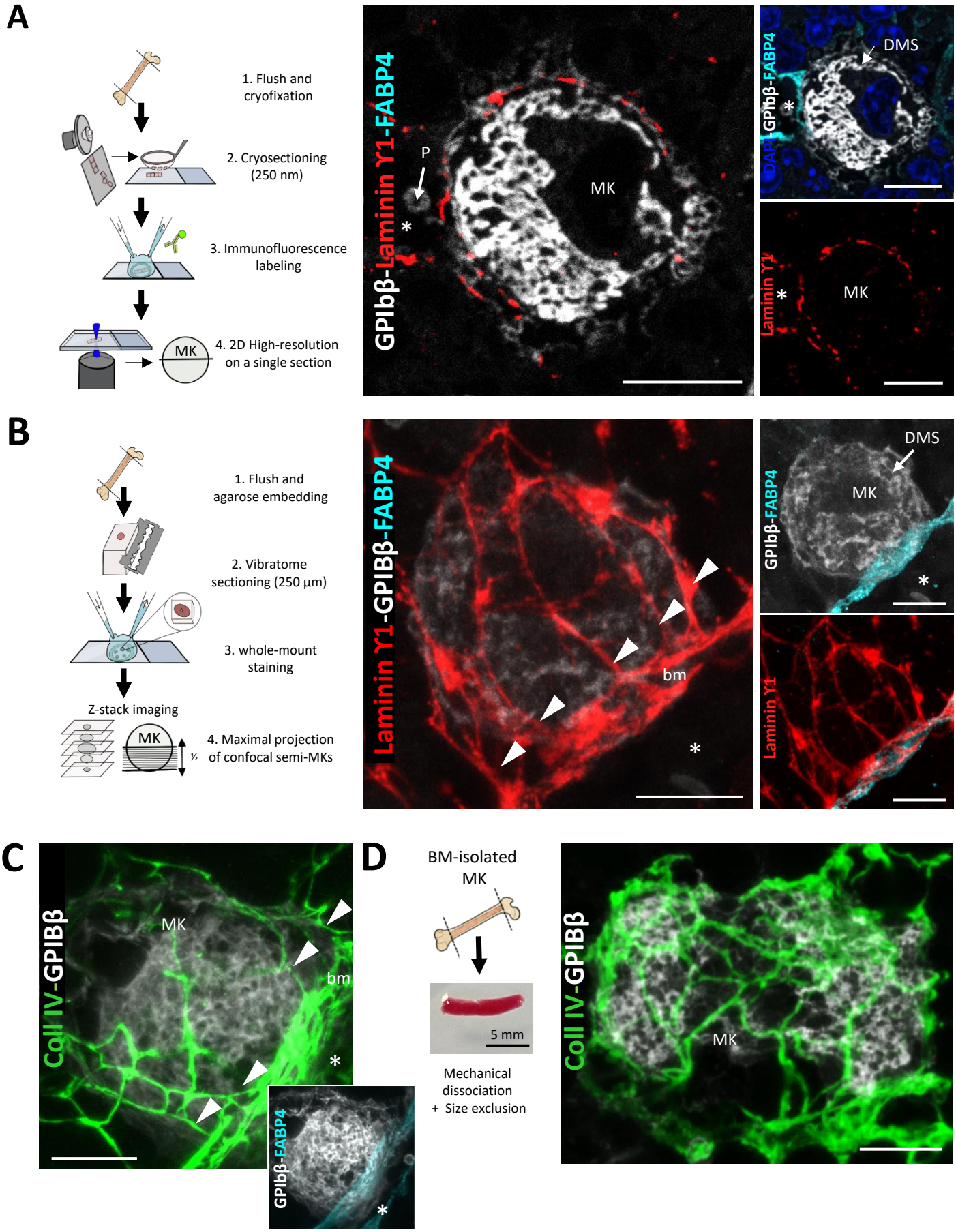
A
1. Flush and cryofixation
2. Cryosectioning (250 nm)
3. Immunofluorescence labeling
MK
4. 2D High-resolution on a single section
GPIbβ-Laminin Y1-FABP4
P
MK
*
DAPI-GPIbβ-FABP4
DMS
Laminin Y1
B
1. Flush and agarose embedding
2. Vibratome sectioning (250 µm)
3. whole-mount staining
Z-stack imaging
MK
½
4. Maximal projection of confocal semi-MKs
Laminin Y1-GPIBβ-FABP4
bm
GPIbβ-FABP4
C
Coll IV-GPIBβ
MK
bm
GPIbβ-FABP4
D
BM-isolated MK
5 mm
Mechanical dissociation
+ Size exclusion
Coll IV-GPIBβ

Figure 1

LaminiΝ1 and collagen IV form 3D cages of ECM for megakaryocytes, directly connected to the sinusoidal basement membrane

(A) Left panel. Schematic representation of the experimental workflow for 2D imaging of immunostained bone marrow cryosections from WT mice. Confocal imaging is performed on single ultrathin sections with an axial resolution of 250 µm. Right panel. Representative 2D images of a sinusoid-associated megakaryocyte immunostained for laminin Ν1 (red), GPIbβ (white) and FABP4 (cyan). Cell nuclei are visualized with DAPI (blue) (from one out of three independent IF experiments).
(B) Left panel. Schematic representation of the experimental workflow for 3D analysis of whole-mount bone marrow preparations from WT mice. A stack of confocal images covering half the depth of the megakaryocyte is acquired and then z-projected to create a maximum projection image. Right panel. Representative maximal projection images of sinusoid-associated megakaryocyte immunostained for laminin Ν1 (red), GPIbβ (white) and FABP4 (cyan) (from one out of three independent IF experiments).
(C) Representative maximal projection images of sinusoid-associated megakaryocyte immunostained for collagen IV (green) and GPIbβ (white). The inset image shows the FABP4 (cyan) and megakaryocyte (white) immunostaining.
(D) Bone marrow-isolated megakaryocyte maintaining an ECM cage. Left panel. Schematic of the experimental procedure used to isolate mouse bone marrow megakaryocytes. Right panel. Maximal projection 3D images showing the persistence of the ECM cage (collagen IV in green) around a freshly isolated megakaryocyte (GPIbβ in white).

*, sinusoid lumen ; arrowheads, basement membrane-cage connections; BM, bone marrow; bm, basement membrane ; MK, megakaryocyte; Bars, 10 µm**.**

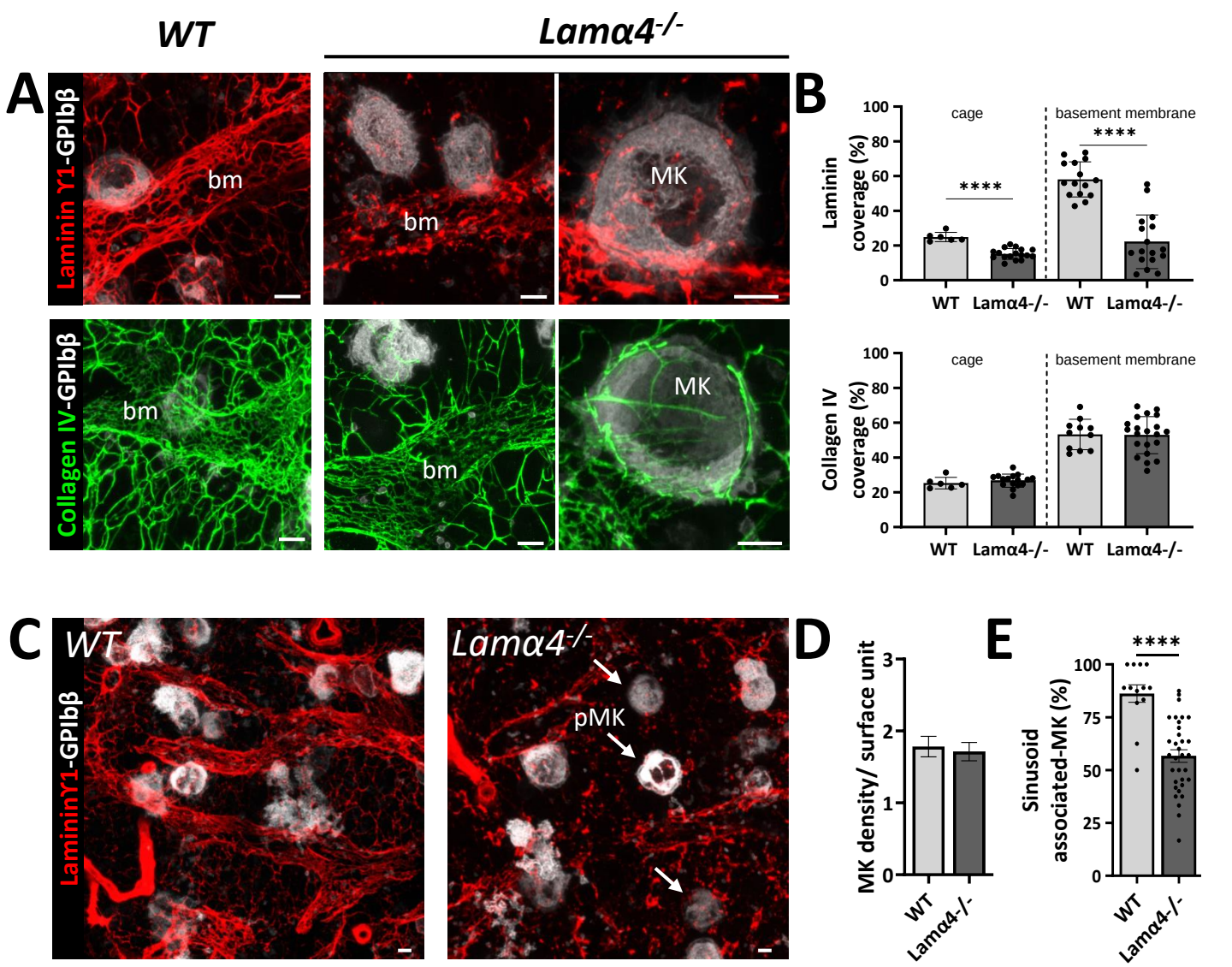

Figure 2

Reduced laminin ϒ1 cage and megakaryocyte-sinusoid interactions in *Lamα4*$^{-/-}$ mouse bone marrow.

(A-B) Depletion of laminin α4 leads to a reduction in the laminin ϒ1 deposition, but not in collagen IV, in the cage around megakaryocytes and in the sinusoid basement membrane.

A. Representative maximal projection images showing the immunostaining of laminin γ1 (red) or collagen IV (green) in the *Lamα4*$^{-/-}$ compared to control mice. Two magnifications are shown for *Lamα4*$^{-/-}$ mouse.

B. Quantification of laminin γ1 and collagen IV surface coverage per megakaryocyte and per basement membrane surface (laminin: 6<cage<17 and 15<bm<17; collagen IV: 6<cage<16 and 11<bm<21 expressed as a percentage, ****P>0.001 unpaired t-Test).

(C-E) Depletion of laminin α4 leads to a decrease in the sinusoid-associated megakaryocytes.

C. Representative maximal projections showing the immunostaining of laminin γ1 (red) and megakaryocytes (GPIbβ in white) in the bone marrow of *Lamα4*$^{-/-}$ and control mice.

D. Quantification of the total number of megakaryocytes per surface unit (s.u., 12,945 µm^2, n=3 for each genotype, 87<n<92, P=0.9228, ns, Mann-Whitney test).

E. Quantification of the sinusoid-associated megakaryocytes (n=3, ****P>0.001 unpaired t-Test) in control (grey) and *Lamα4*$^{-/-}$ (dark) mice. Arrows point to megakaryocytes which are not associated with sinusoids (pMK).

bm, basement membrane; MK, megakaryocyte; pMK, MK in the parenchyma; Bar, 10 µm.

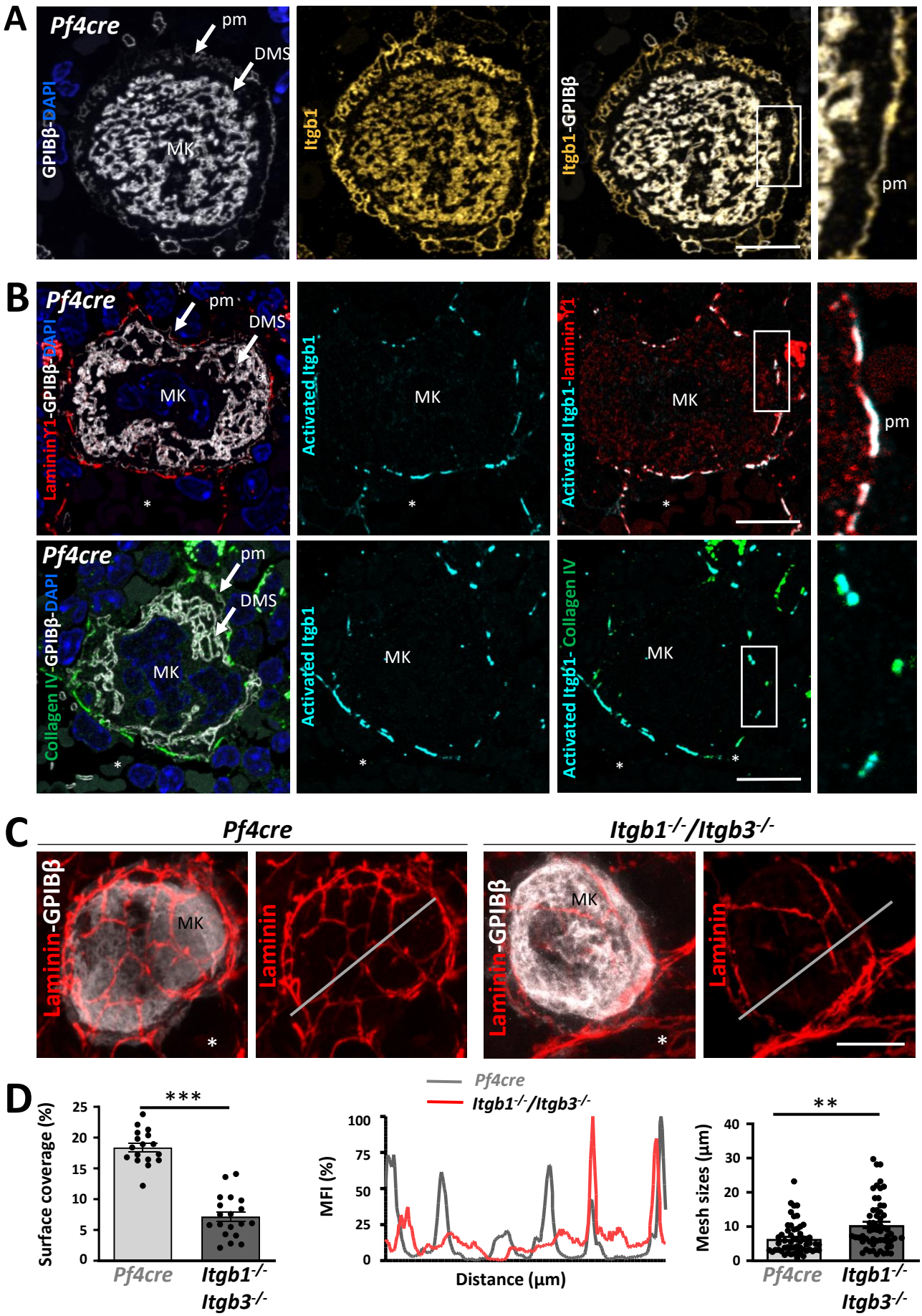
A
Pf4cre
pm
DMS
MK
GPIBβ-DAPI
Itgb1
Itgb1-GPIBβ
pm
B
Pf4cre
pm
DMS
MK
LamininY1-GPIBβ-DAPI
Activated Itgb1
MK
Activated Itgb1-laminin Y1
MK
pm
Pf4cre
pm
DMS
MK
Collagen IV-GPIBβ-DAPI
Activated Itgb1
MK
Activated Itgb1- Collagen IV
MK
C
Pf4cre
Itgb1-/-/Itgb3-/-
Laminin-GPIBβ
MK
Laminin
Laminin-GPIBβ
MK
Laminin
D
Surface coverage (%)
***
Pf4cre
Itgb1-/-
Itgb3-/-
Pf4cre
Itgb1-/-/Itgb3-/-
MFI (%)
Distance (µm)
Mesh sizes (µm)
**
Pf4cre
Itgb1-/-
Itgb3-/-

Figure 3

Integrin-mediated control of the 3D ECM cage around megakaryocytes

(A) Representative 2D images of *Pf4cre* bone marrow cryosections (250 nm) showing a sinusoid-associated megakaryocyte immunostained for β1 integrin (MAB1997 in yellow). Right: the boxed area is shown at a higher magnification.
(B) Activated β1 integrins form functional adhesion structures around megakaryocyte surfaces. Representative 2D images of *Pf4cre* bone marrow cryosections showing laminin (red, upper panels) or collagen IV (green, lower panels) staining around a sinusoid-associated megakaryocyte immunostained for activated β1 integrin (9EG7 in cyan) and GPIbβ (white). Right: Magnification of the boxed area showing co-localization of the ECM proteins and activated β1 integrin.
(C) Depletion of β1 and β3 integrins leads to a reduction in the laminin deposition on the surface of megakaryocytes. Representative 3D images showing a decrease in laminin deposition (red) on *Itgb1*$^{-/-}$/*Itgb3*$^{-/-}$ megakaryocytes compared to *Pf4cre.*
(D) Quantification of laminin surface coverage per megakaryocyte (in %, 17<n<19 as indicated in the bars, ***P>0.001 unpaired t-Test), (Middle) expression profile of the laminin staining along straight-lines (25 µm long) visible as white lines in the confocal images, and (Right) quantification of mesh sizes (in µm, 14<n<16, **P<0.01 Mann-Whitney).

*, sinusoid lumen; MFI, mean fluorescence intensity; MK, megakaryocyte; pm, plasma membrane; Bars, 10 µm.

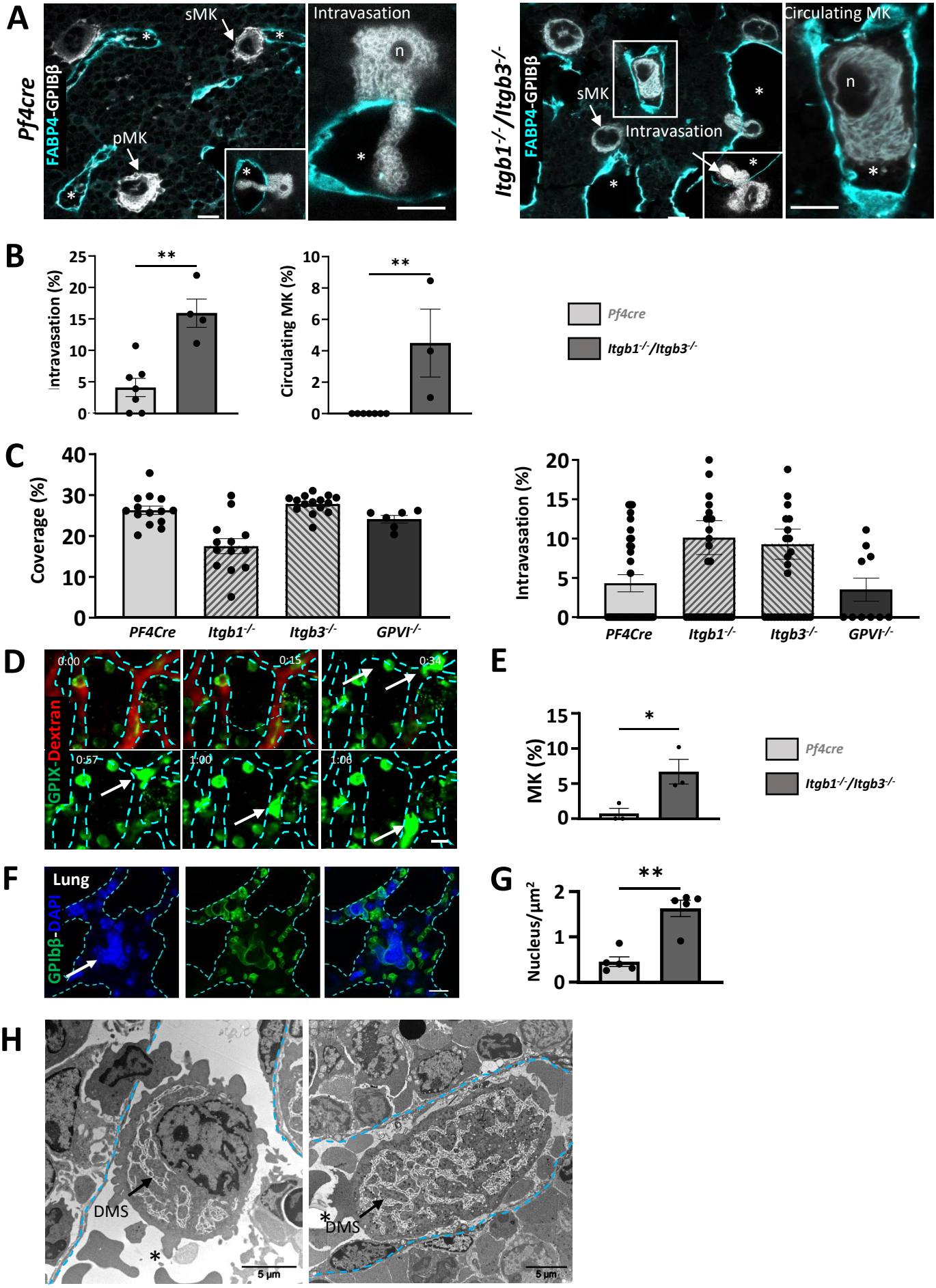
A
Pf4cre
FABP4-GPIBβ
sMK
pMK
Intravasation
n
Itgb1-/-/Itgb3-/-
Circulating MK
B
Intravasation (%)
Circulating MK (%)
**
Pf4cre
Itgb1-/-/Itgb3-/-
C
Coverage (%)
Intravasation (%)
PF4Cre
Itgb1-/-
Itgb3-/-
GPVI-/-
D
GPIX-Dextran
0:00
0:15
0:34
0:57
1:00
1:06
E
MK (%)
*
F
Lung
GPIbβ-DAPI
G
Nucleus/μm²
H
DMS
5 μm

Figure 4

Integrins protects megakaryocytes from entering the bloodstream as whole cells

(A-C)) Higher proportion of intravasation events in mice lacking β1/β3 integrins.

A. Representative confocal images of *Pf4cre* and *Itgb1*$^{-/-}$/*Itgb3*$^{-/-}$ whole-mount bone marrow immunostained for GPIbβ (white) and FABP4 (cyan).

B. Quantification of megakaryocyte intravasation and circulating megakaryocytes (3 mice minimum for each genotype, 213<n<397 for Pf4cre and *Itgb1*$^{-/-}$/*Itgb3*$^{-/-}$, ** P<0.001 Mann Whitney).

C. Quantification of the laminin γ1 deposition in the ECM cage in single knockout integrins and in GPVI knockout**.** Quantification of the intravasation events in single knock-out mice showing that both integrins are essential for the proper anchoring of megakaryocytes in their vascular niche.

(D -E) Intravital two-photon imaging of *Itgb1*$^{-/-}$/*Itgb3*$^{-/-}$ mouse calvarial bone marrow

D. Tissues were stained with intravenously injected AF488-conjugated anti-GPIX antibody and rhodamin dextran**.** The white arrow indicates an intrasinusoidal *Itgb1*$^{-/-}$/*Itgb3*$^{-/-}$ megakaryocyte, dotted lines illustrate the sinusoid wall and the values in the left corner show the time-lapses.

E. Quantification of circulating megakaryocytes, expressed as a percentage of the total number of megakaryocyte (from 3 independent experiments, 130<n<136, 0.0279 *P<0.1, Paired t-test).

(F-G) Large megakaryocyte nuclei detected in the pulmonary capillaries of *Itgb1*$^{-/-}$/*Itgb3*$^{-/-}$ mice

F. Representative confocal images showing megakaryocytes' nucleus (arrow, GPIbβ green, DAPI nucleus) within the pulmonary microvessels of *Itgb1*$^{-/-}$/*Itgb3*$^{-/-}$ mice**.** Cyan dotted lines indicate the vessel wall.

G. Quantification of the intravascular megakaryocytes (from 5 independent experiments, 28<n<149, 0.0079 ***P*<0.01, Mann-Whitney).

(H) Two TEM image showing intravascular entire *Itgb1*$^{-/-}$/*Itgb3*$^{-/-}$ megakaryocyte.

*, sinusoid wall; FG, fibrinogen; FN, fibronectin; FG, fibrinogen; n, nucleus; sMK, sinusoid-associated MK; pMK, MK in the parenchyma; PPT, proplatelets; Bars in A-G, 10 µm; Bar in E, 5 µm; Bar in G, 30µm.

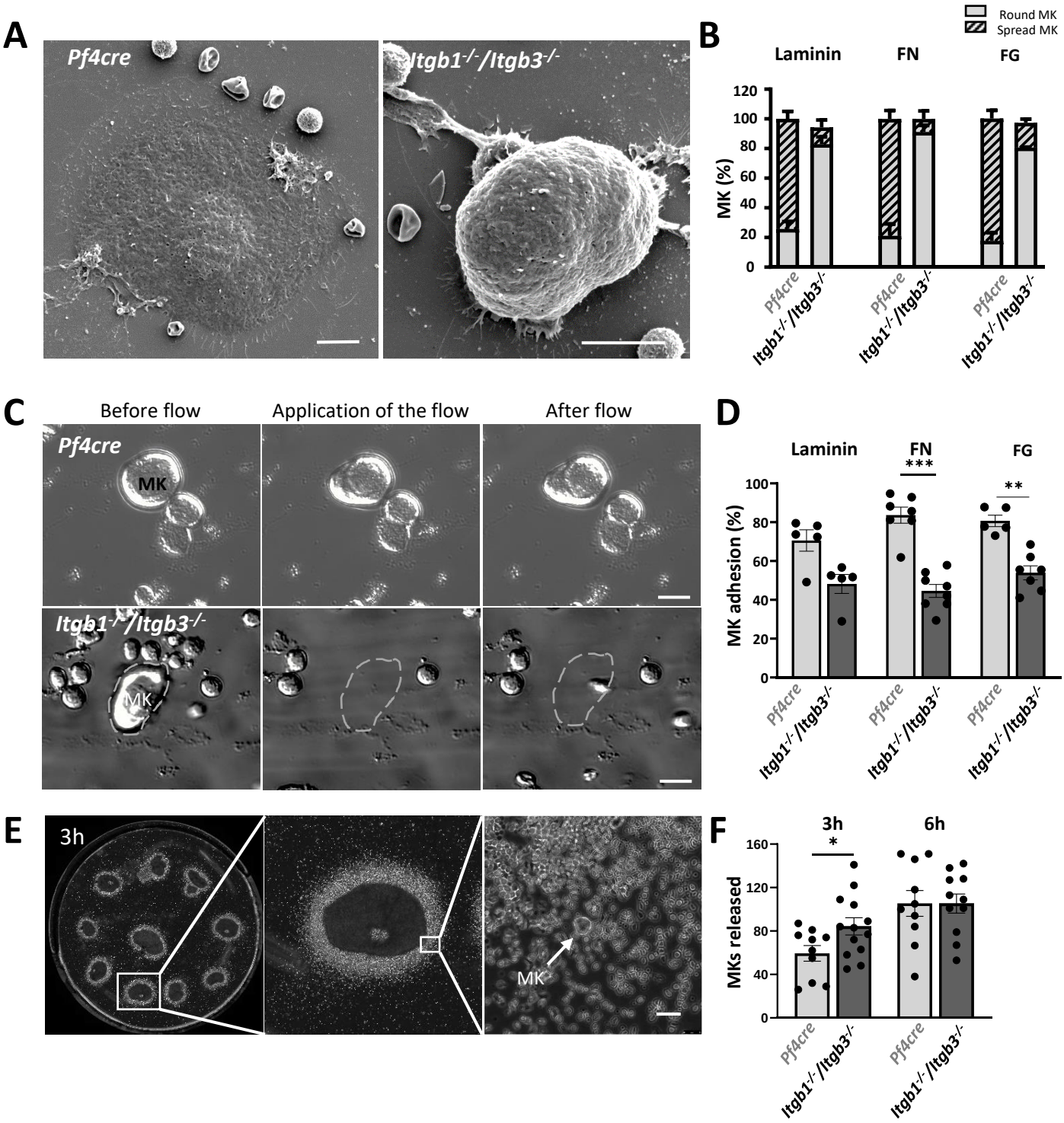
A
Pf4cre
Itgb1-/-/Itgb3-/-
B
Round MK
Spread MK
Laminin
FN
FG
MK (%)
120
100
80
60
40
20
0
Pf4cre
Itgb1-/-/Itgb3-/-
C
Before flow
Application of the flow
After flow
Pf4cre
MK
Itgb1-/-/Itgb3-/-
MK
D
Laminin
FN
FG
***
**
MK adhesion (%)
100
80
60
40
20
0
Pf4cre
Itgb1-/-/Itgb3-/-
E
3h
MK
F
3h
6h
*
MKs released
160
120
80
40
0
Pf4cre
Itgb1-/-/Itgb3-/-

Figure 5

Integrins promote megakaryocyte adhesion to the ECM components of the bone marrow

(A-B) Impaired adhesion and spreading of *Itgb1$^{-/-}$/Itgb3$^{-/-}$* megakaryocytes.

A. Representative SEM images depicting bone marrow-derived megakaryocytes adhering on laminin.

B. Spreading (hatched bars) and round (grey bars) megakaryocytes were counted following 3h incubation on laminin, fibronectin (FN), and fibrinogen (FG) (in %) (from 4-6 independent experiments).

(C-D) Microfluidic flow chamber to study megakaryocyte adhesion efficiency.

C. Representatives bright field images showing that upon flow application, *Itgb1$^{-/-}$/Itgb3$^{-/-}$* megakaryocytes detach from fibrillary fibronectin protein, while *Pf4Cre* MKs remain attached.

D. Quantification of the detachment of *Pf4cre* and *Itgb1$^{-/-}$/Itgb3$^{-/-}$* megakaryocytes on laminin, fibrillar fibronectin and fibrinogen (from 5 to 7 independent experiments ,**P<0.01, ***P<0,001, Mann-Whitney).

(E-F) Reduced physical anchoring of *Itgb1$^{-/-}$/Itgb3$^{-/-}$* megakaryocytes to bone marrow.

E. Representatives bright field images of the ten femur bone marrow sections placed in an incubation chamber (left panel), of the box (center panel) and of the megakaryocytes released from the periphery of the explants (right panel).

F. Quantification of the number of *Pf4cre* and *Itgb1$^{-/-}$/Itgb3$^{-/-}$* megakaryocytes released from the explants following 3h (from 10 to 13 independent experiments, 594<n<1095 for Pf4cre and *Itgb1$^{-/-}$/Itgb3$^{-/-}$*, *P<0.05, unpaired t-test).

dotted lines, MK detachment; MK, megakaryocytes, FN, fibronectin; FG, fibrinogen; n, number of cells studied; Bars in A, 10 µm; Bars in B, 20 µm; Bars in B, 30 µm.

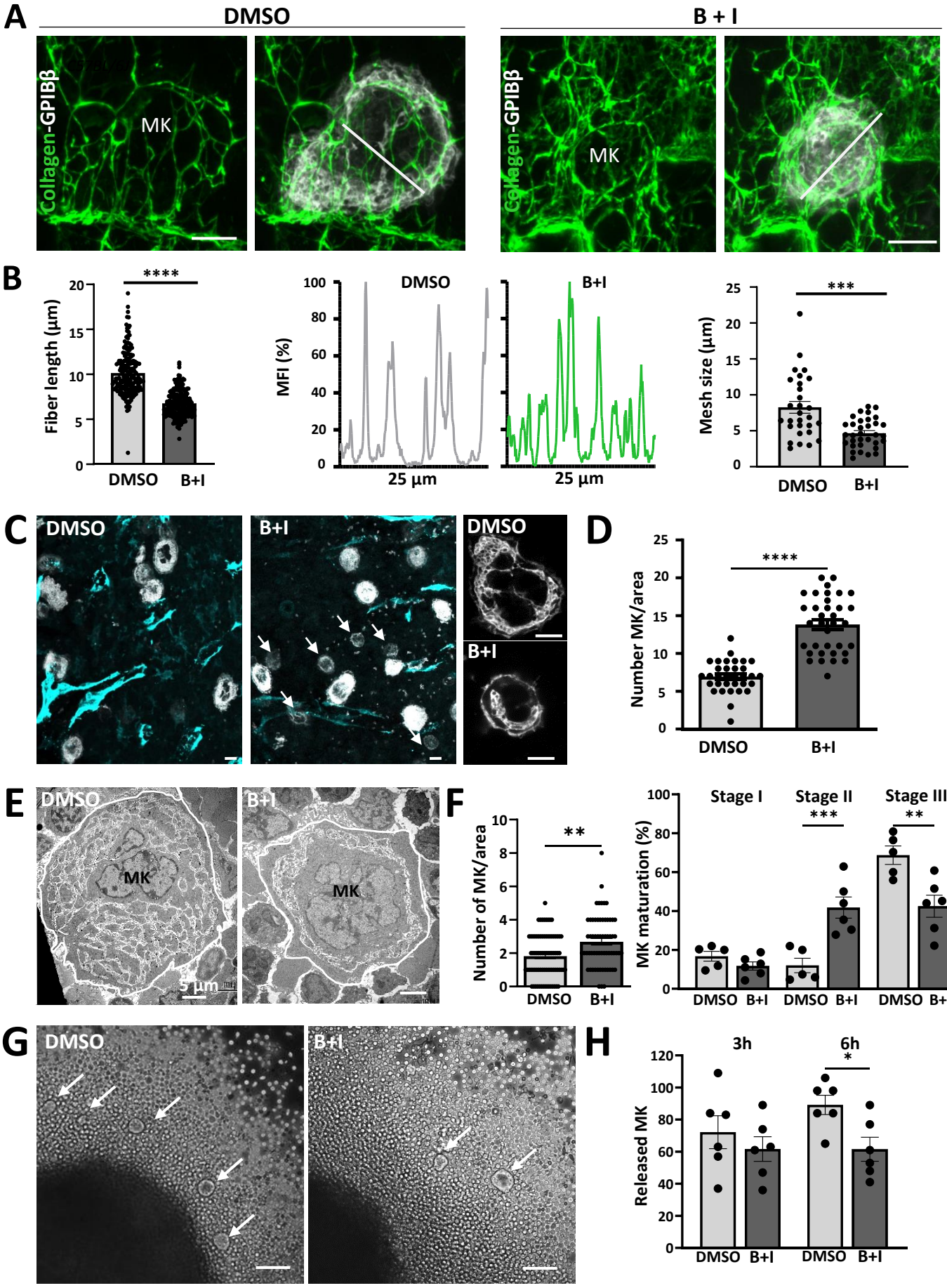
A
DMSO
B + I
Collagen-GPIBβ
MK
Collagen-GPIBβ
MK
B
Fiber length (µm)
****
DMSO
B+I
MFI (%)
DMSO
B+I
25 µm
25 µm
Mesh size (µm)
***
DMSO
B+I
C
DMSO
B+I
DMSO
B+I
D
Number MK/area
****
DMSO
B+I
E
DMSO
B+I
MK
MK
5 µm
F
Number of MK/area
**
DMSO
B+I
MK maturation (%)
Stage I
Stage II
Stage III
***
**
DMSO
B+I
DMSO
B+I
DMSO
B+I
G
DMSO
B+I
H
Released MK
3h
6h
*
DMSO
B+I
DMSO
B+I

Figure 6

Maturation of the 3D ECM cage is correlated with maturation of the DMS in megakaryocytes

(A-B) MMP inhibition leads to a densification of the 3D ECM cage.

A. Representative 3D confocal images showing a significant increase in collagen IV deposition (green) on the megakaryocyte surface in treated mice treated with the intravenous cocktail of protease inhibitors (B + I).

B. (Left) Quantification of collagen IV fluorescence showed a shortening of collagen IV fibers in treated mice compared to that in control mice (from 3-5 independent experiments, 20<n<22 as indicated in the bars, ****P<0;001, Mann-Whitney), (Middle) Histograms of fluorescence intensity versus distance showed an increase in cross-linking with a reduction in pore size (white lines of 25µm length are visible in the confocal images), (Right) Reduction in mesh sizes in treated mice (from 3 independent experiments, 7<n<12, ***P>0.001, t-test).

(C-D) MMP inhibition affects megakaryocyte growth.

C. Representative confocal images from DMSO *vs* B+I treated mice immunostained for GPIbβ (white) and FABP4 (cyan), zoomed-in images showing the difference in megakaryocyte size between the two groups (arrows).

D. Quantification of the number of megakaryocytes per bone marrow area (194 x 194 µm) (from 3 independent experiments, 229<n<483 as indicated in the bars, ****P<0.0001, Mann-Whitney).

(E-F) MMP inhibition leads to an increased in the number of immature megakaryocytes.

E. TEM observation revealed the presence of numerous immature megakaryocytes (stage II) in treated mice as compared to fully mature megakaryocytes in control mice (stage III).

F. Quantification of the total number of megakaryocytes (145<n<169 as indicated in bars, **P<0.01, Mann-Whitney) and in the proportion of immature megakaryocytes (stage II) in the B + I group (from 3 independent experiments, **P < 0.05, ***P < 0.01, one way ANOVA with Tukey correction).

(G-H) MMP inhibition reduced release of megakaryocytes from the bone marrow explant.

G. Representatives bright field images of the megakaryocytes (arrows) released from the periphery of the control and treated explants.

H. Quantification of the number of megakaryocytes released following 3h and 6h (from 6 independent experiments, 369<n<783 for DMSO and B+I, *P<0.05, unpaired t-test).

B + I, batimastat + Ilomastat; sMK, sinusoid-associated MK; pMK, MK in the parenchyma; n, number of cells studied; Bars in A and C, 10 µm; Bars in E, 5 µm; Bar in G, 50 µm.

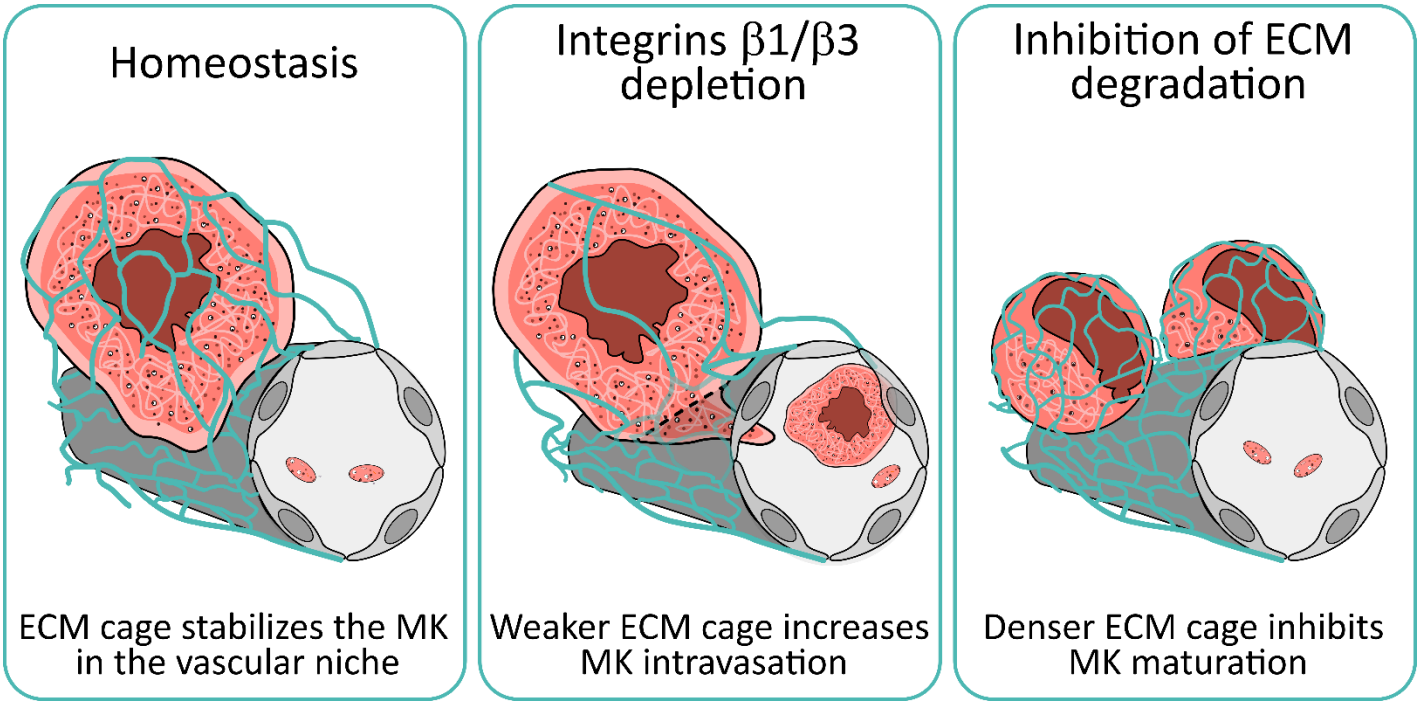

Figure 7

Integrin-mediated signaling and MMP proteolysis regulate the matrix remodeling and the adhesive properties of the 3D ECM cage, which control megakaryocyte maturation and intravasation at the bone marrow-blood interface.

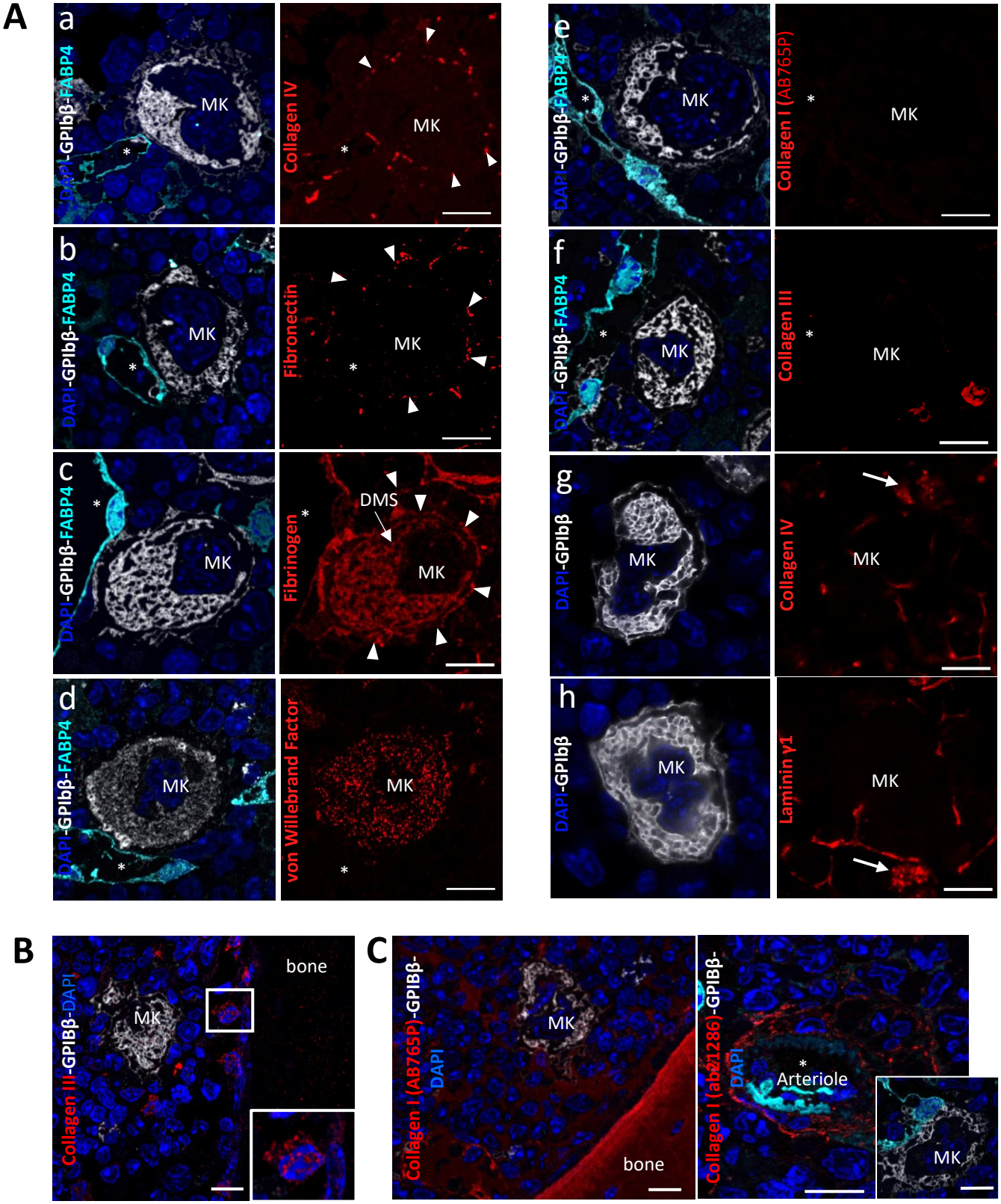
A
a
DAPI-GPIbβ-FABP4
MK
Collagen IV
b
Fibronectin
c
Fibrinogen
DMS
d
von Willebrand Factor
e
Collagen I (AB765P)
f
Collagen III
g
h
Laminin γ1
B
Collagen III-GPIBβ-DAPI
bone
C
Collagen I (AB765P)-GPIBβ-DAPI
Collagen I (ab21286)-GPIBβ-DAPI
Arteriole

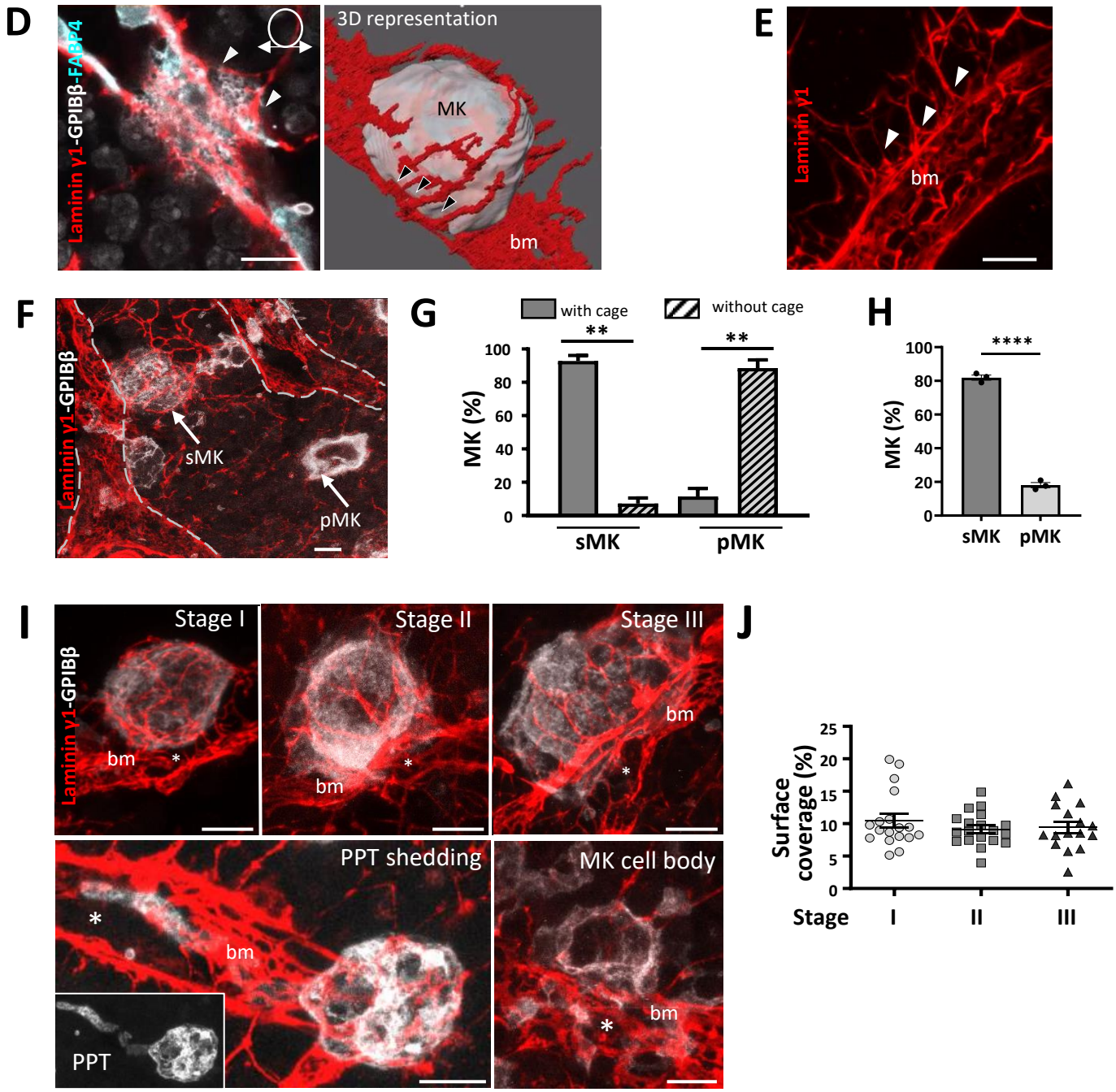
D
Laminin γ1-GPIBβ-FABP4
3D representation
MK
bm
E
Laminin γ1
bm
F
Laminin γ1-GPIBβ
sMK
pMK
G
with cage
without cage
MK (%)
sMK
pMK
H
MK (%)
sMK
pMK
I
Laminin γ1-GPIBβ
Stage I
Stage II
Stage III
bm
PPT shedding
MK cell body
PPT
J
Surface coverage (%)
Stage
I
II
III
K
FABP4-GPIBβ
MK
Fibronectin
bm
FABP4-GPIBβ
MK
fibrinogen
bm

Supplemental Figure 1

Molecular cartography of the ECM around megakaryocytes.

(A) Immunofluorescence 2D analysis of ECM proteins. Collagen IV (a and g), laminin γ1 (h), fibronectin (b), fibrinogen (c), von Willebrand factor (d), and collagen I /III (e-f) around sinusoid-associated megakaryocytes. Bone marrow immunostained for GPIbβ(white), FABP4 (cyan), and DAPI (blue).

(B) Positive immunostaining of small stromal cells near the bone with the antibody against collagen III.

(C) Positive immunostaining of the bone and arterioles using two antibody against collagen I (AB765P and ab21286, respectively). Note that the megakaryocytes are not immunostained.

(D-E) Direct connections between the basement membrane and the ECM cage

D. Maximal projection showing the interface between the basement membrane (red), the sinusoid (blue) and megakaryocyte (white). The next image is a 3D reconstruction of this area.

E. Maximum projection of 3D laminin ϒ1 fibers linked to the basement membrane. The arrowheads indicate the connextion between the basement membrane and the cage.

(F-H) The spatial distribution of the ECM cage is highly restrictive to the sinusoid-associated megakaryocytes

F. Maximal projection of a large field of the 3D laminin ϒ1 organization. Megakaryocytes in contact with sinusoids (sMK) have a cage, while megakaryocytes in the parenchyma (pMK) were surrounded by sparse interstitial laminin ϒ1. Bone marrow immunostained for GPIbβ(white) and laminin ϒ1 (red).

G. Quantification of the number of megakaryocytes displaying the typical 3D cage as a function of cell association with sinusoids**.** Megakaryocytes with an ECM cage (grey bars) and without a cage (hatched bars) were counted (three complete 3D stacks from independent mice, 126 megakaryocytes counted in total as indicated in the bars, **P<0.01 Mann-Whitney).

H. Quantification of the pMK relative to the total MK population. Megakaryocytes in the stroma and in contact with sinusoids were counted on three complete 3D stacks from independent mice, ***P<0.0001, unpaired t-test). OK

(I-J) Correlation with the maturation stages of megakaryocytes.

I. Maximal projections of megakaryocytes are shown. Bone marrow immunostained for GPIbβ(white) and laminin ϒ1 (red).

J. Quantification of laminin γ1 immunostaining on megakaryocytes. Quantification per cell shows the presence of a 3D ECM cage at all stages of maturation (2-3 independent experiments, 14<n<22 as indicated in the bars, *P<0,05 Mann-Whitney). Quantification on megakaryocytes extending proplatelets and residual megakaryocytes was not possible due to sample size limitations.

(K) Distribution of fibronectin and fibrinogen around sinusoid-associated megakaryocytes. Maximal projection 3D images showing the absence of ECM connections with the basement membrane for fibronectin (magenta) and fibrinogen (yellow). Sinusoid endothelial cells were visualized with anti-FABP4 (cyan) and megakaryocytes were identified with anti-GPIbβ (white).

Arrowheads, peri-MK staining; Arrow, staining in adjacent small cells in (Ag-h); bm, basement membrane; MK, megakaryocyte; DMS, demarcation membrane system; PPT, proplatelet; *, vascular lumen; Bar, 10 µm**.**

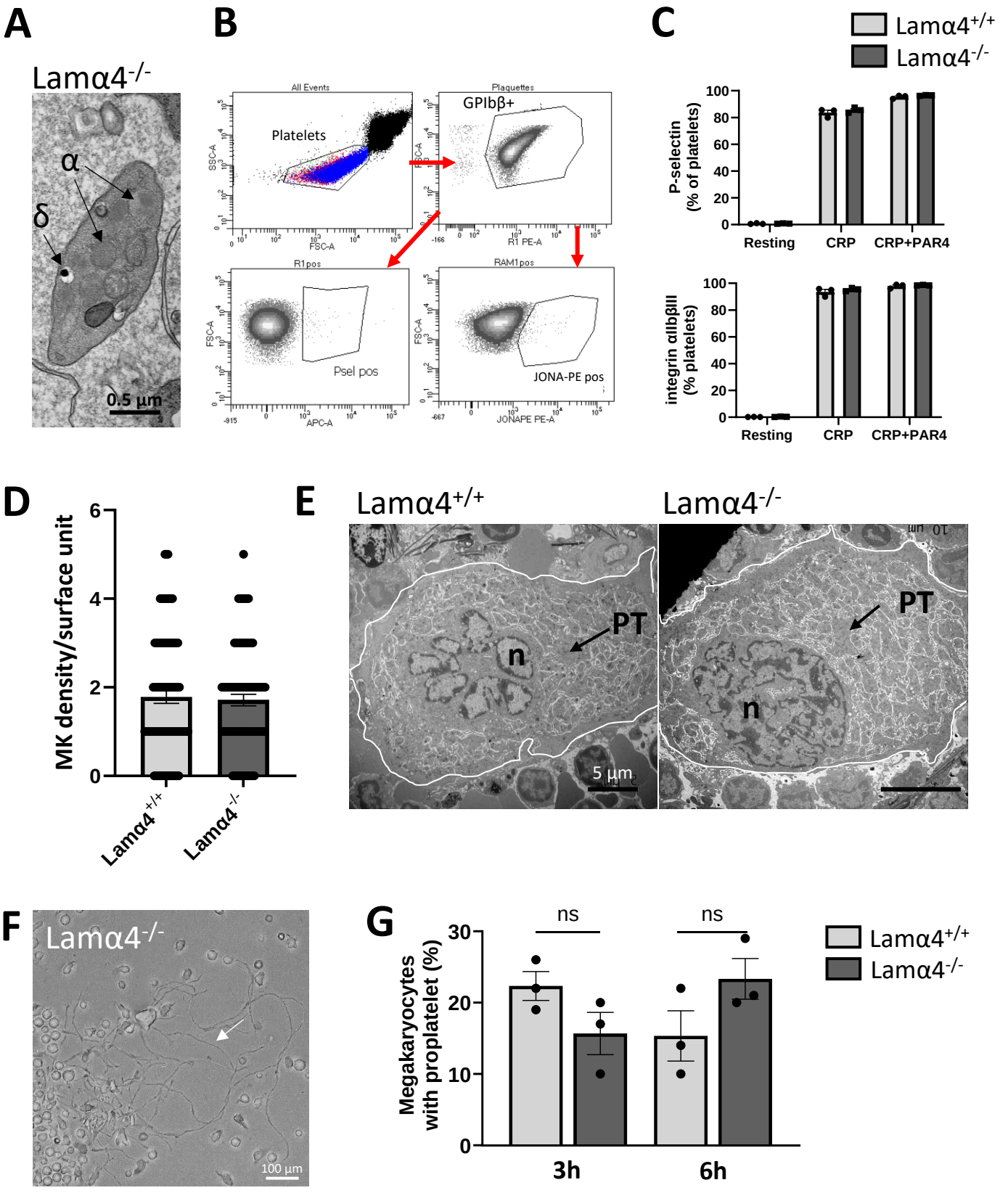
A
Lamα4-/-
α
δ
0.5 µm
B
All Events
Platelets
SSC-A
FSC-A
Plaquettes
GPIbβ+
R1 PE-A
R1pos
Psel pos
APC-A
RAM1pos
JONA-PE pos
JONAPE PE-A
C
Lamα4+/+
Lamα4-/-
P-selectin (% of platelets)
Resting
CRP
CRP+PAR4
integrin αIIbβIII (% platelets)
D
MK density/surface unit
Lamα4+/+
Lamα4-/-
E
Lamα4+/+
Lamα4-/-
PT
n
5 µm
F
Lamα4-/-
100 µm
G
Megakaryocytes with proplatelet (%)
ns
3h
6h
Lamα4+/+
Lamα4-/-

Supplementary Figure 2

Characterization of Lamα4$^{-/-}$ platelets and megakaryocytes

(A-C) Lamα4$^{-/-}$ platelet morphology and functions.

A. Normal size, discoid shape and ultrastructure of Lamα4$^{-/-}$ platelets. Bar: 0.5 µm.

B. Gating strategy for platelet function analysis. Flow cytometry was used to analyse the functions of Lamα4-/- platelets. Following activation with collagen-related peptide (CRP)(40 µg/ml) or CRP + TRAP (4 mM), the expression of P-selectin (CD62P, a marker of α-granule secretion) and P-selectin (JON-A PE, a marker of integrin αIIbβ3 activation) was analyzed.

C. Quantification of the percentage of positive platelets, Bars are the mean ± standard error of the mean (SEM) of 3 to 6 independent experiments. The results were statistically compared to those of control platelets (*P < 0.05; **P < 0.01; ***P < 0.001).

(D-E) Megakaryopoiesis in Lamα4$^{-/-}$ mice.

D. Quantification of the bone marrow megakaryocytes observed by electron microscopy, per surface unit (s.u., 12,945 µm^2). ns, p=0,7177 unpaired t test.

E. Representative TEM images of Lamα4$^{+/+}$ and Lamα4$^{-/-}$ megakaryocytes. Bars, 5 µm.

(F-G) Ex vivo capacity of of Lamα4$^{-/-}$ megakaryocytes to form proplatelets.

F. Representative image showing proplatelets forming-Lamα4$^{-/-}$ megakaryocytes in fresh bone marrow explants. Arrowhead pointes to proplatelets. Scale Bar, 100 µm.

G. Quantification of the percentage of Lamα4$^{+/+}$ and Lamα4$^{-/-}$ megakaryocytes extending proplatelets following 3h and 6h h. Bars represent the mean ± SEM of three independent experiments **(**107<n<113 for Lamα4$^{+/+}$ and Lamα4$^{-/-}$, ns p>0.1, unpaired t-test).

α, alpha granules, δ, dense granules, PT, platelet territories, bm, basement membrane, MK, megakaryocyte*, sinusoid lumen. Bars, 10 µm.

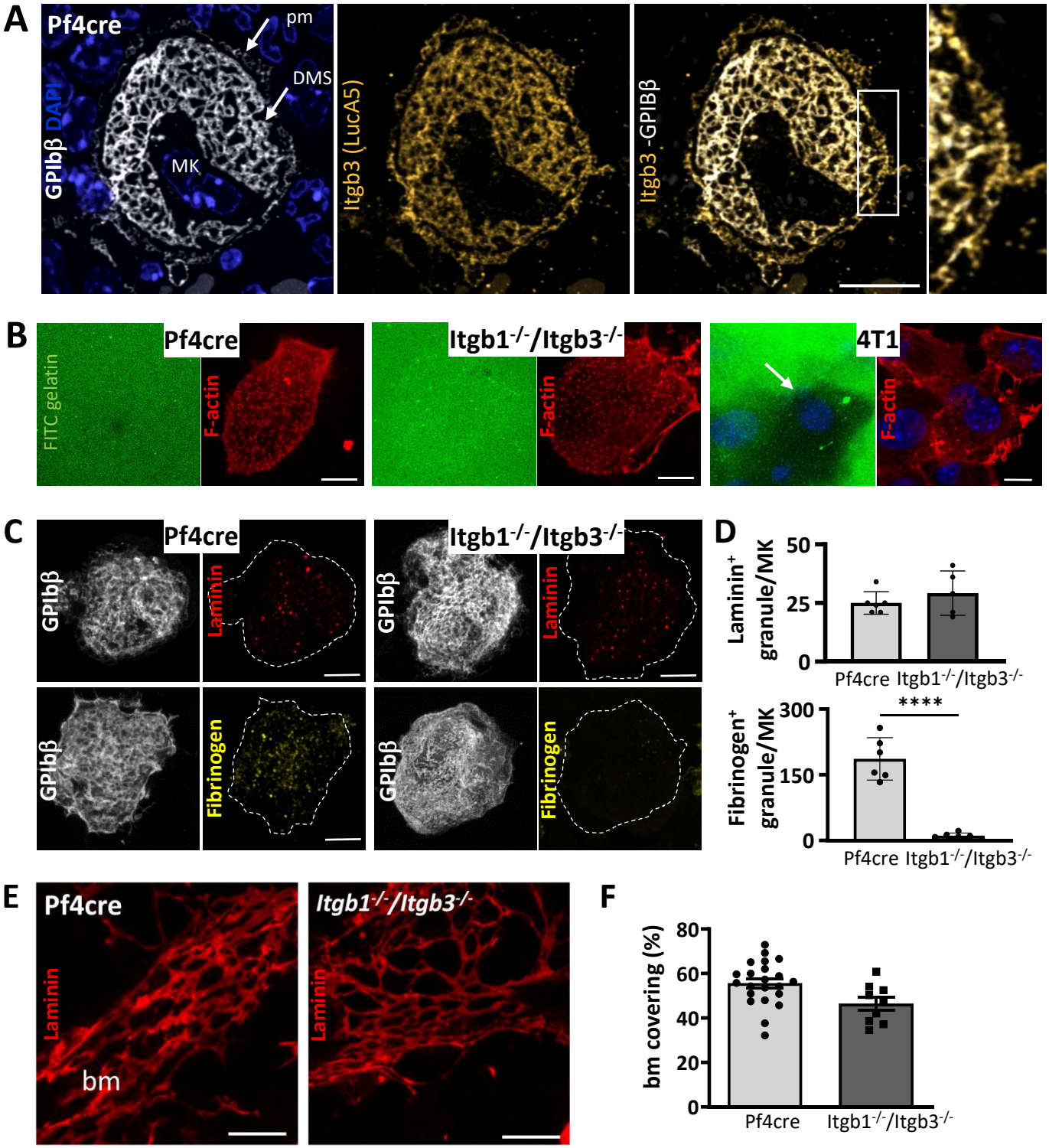
A
Pf4cre
pm
DMS
MK
GPIbβ DAPI
Itgb3 (LucA5)
Itgb3 -GPIBβ
B
Pf4cre
FITC gelatin
F-actin
Itgb1-/-/Itgb3-/-
F-actin
4T1
F-actin
C
Pf4cre
GPIbβ
Laminin
GPIbβ
Fibrinogen
Itgb1-/-/Itgb3-/-
GPIbβ
Laminin
GPIbβ
Fibrinogen
D
Laminin+ granule/MK
50
25
0
Pf4cre
Itgb1-/-/Itgb3-/-
Fibrinogen+ granule/MK
300
150
0
****
Pf4cre
Itgb1-/-/Itgb3-/-
E
Pf4cre
Laminin
bm
Itgb1-/-/Itgb3-/-
Laminin
F
bm covering (%)
80
60
40
20
0
Pf4cre
Itgb1-/-/Itgb3-/-

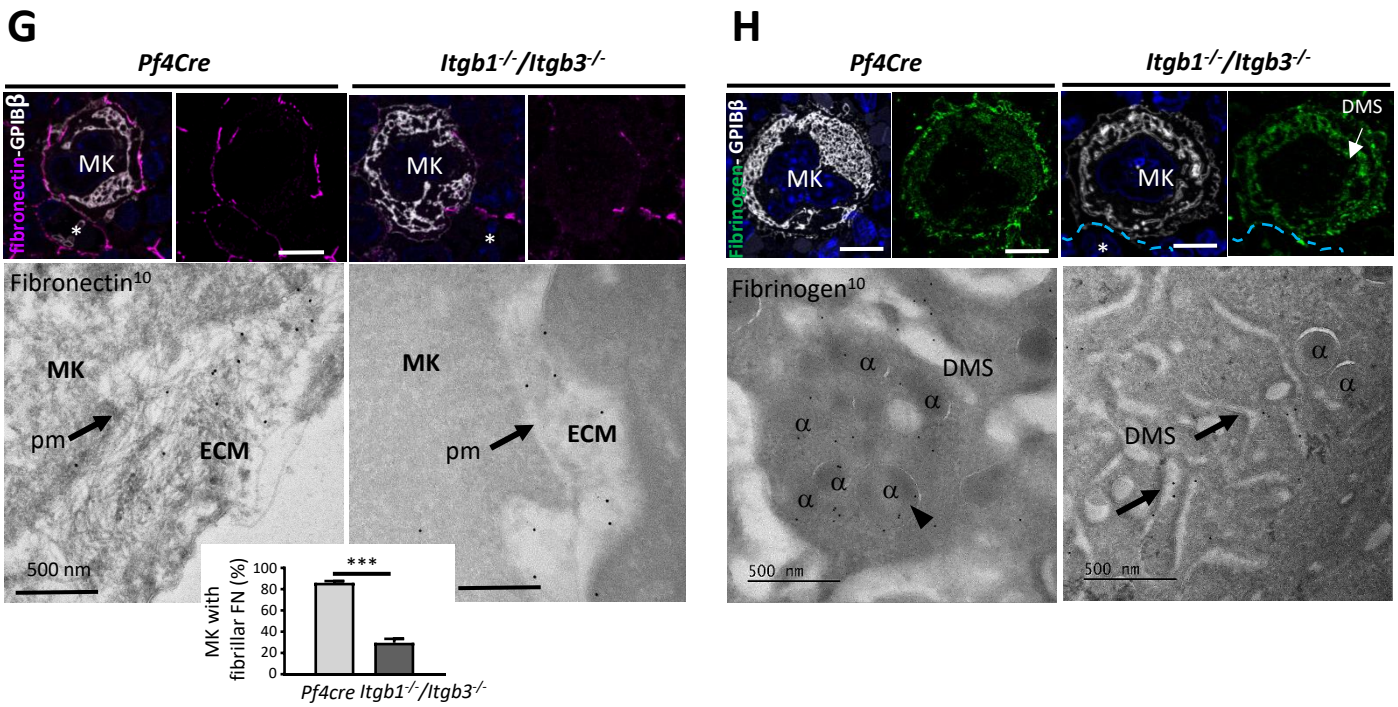

Supplementary Figure 3

Integrins control the structural properties of the ECM cages around megakaryocytes

(A) Representative 2D images of sinusoid-associated megakaryocyte immunostained for β3 integrin (LucA5 in yellow). Right panel: the boxed area is shown at a higher magnification.

(B) Itgb1$^{-/-}$/Itgb3$^{-/-}$ megakaryocytes did not display enhanced degradation of gelatin matrix. Freshly isolated megakaryocytes from Pf4cre or Itgb1$^{-/-}$/Itgb3$^{-/-}$ bone marrow were deposited on a fluorescent gelatin matrix (green) for 3h and labeled with phalloidin (adhesive structures in red). ECM degradation was virtually absent in Pf4cre and Itgb1$^{-/-}$/Itgb3$^{-/-}$ megakaryocytes. Tumoral 4T1 cells, which trigger large dark digested areas (arrow), were used as a positive control.

(C-D) Laminin is present in similar amounts in Itgb1$^{-/-}$/Itgb3$^{-/-}$ and Pf4cre megakaryocytes.

C. Maximal projection 3D images illustrating the presence or not of granules containing laminin (in red) and fibrinogen (in yellow, as negative control) in megakaryocytes (in white) from freshly isolated Pf4cre and Itgb1$^{-/-}$/Itgb3$^{-/-}$ megakaryocytes. The dotted lines delineated megakaryocytes.

D. Quantification of the number of granules per megakaryocyte (5<MK<6, ****P>0.001, t-test).

(E-F) Normal laminin deposition in the sinusoid basement membrane in Itgb1$^{-/-}$/Itgb3$^{-/-}$

E. Representative 3D images of basement membrane immunostained for laminin ϒ1 (red) (from one out of three independent IF experiments).

F. Quantification of fluorescence intensity of laminin per basement membrane surface (expressed as a percentage).

(G-H) Fibronectin and fibrinogen failed to form a ECM cage around Pf4cre and Itgb1$^{-/-}$/Itgb3$^{-/-}$ megakaryocytes

G. Decrease in the expression of fibrillar fibronectin around Itgb1$^{-/-}$/Itgb3$^{-/-}$ megakaryocytes.

H. Mislocalization of fibrinogen in Itgb1$^{-/-}$/Itgb3$^{-/-}$ megakaryocytes.

Top panels. 2D immunofluorescence of Pf4cre and Itgb1$^{-/-}$/Itgb3$^{-/-}$ bone marrow cryosections using anti-fibronectin (magenta) and anti-fibrinogen (green) antibodies.

Lower panels ImmunogoldEM images showing the fibronectin and fibrinogen stainings with 10 nm gold particles. Without integrins, megakaryocytes are unable to effectively remodel fibronectin into fibers. Fibrinogen staining is located in the α granules of Pf4cre megakaryocytes and retained in the extracellular DMS space of Itgb1$^{-/-}$/Itgb3$^{-/-}$ megakaryocytes.

α, alpha granules; arrowheads, peri-MK staining; bm, basement membrane; MK, megakaryocyte; pm, plasma membrane; *, sinusoid lumen; Bar, 10 µm.

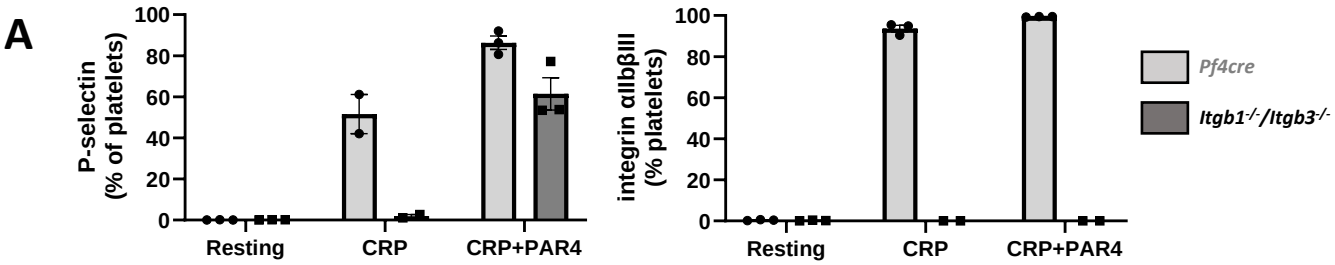
A
P-selectin (% of platelets)
integrin αIIbβIII (% platelets)
Resting
CRP
CRP+PAR4
Pf4cre
Itgb1-/-/Itgb3-/-

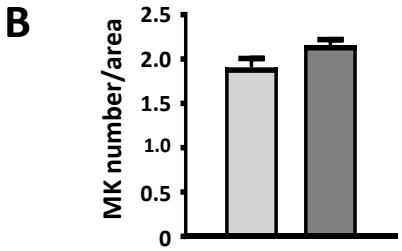
B
MK number/area

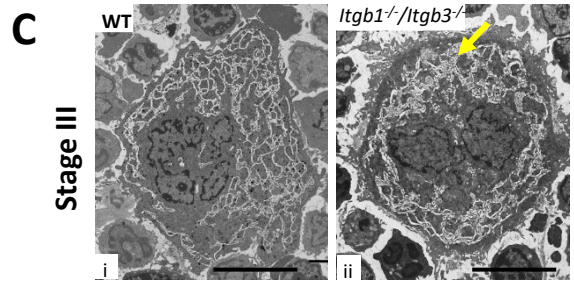
C
Stage III
WT
Itgb1-/-/Itgb3-/-
i
ii

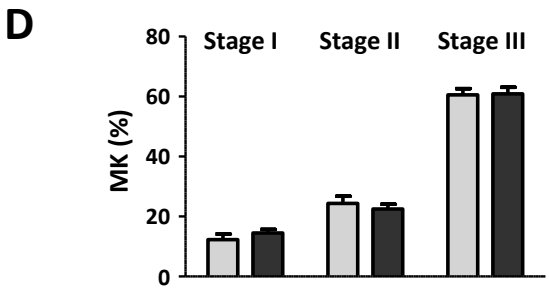
D
MK (%)
Stage I
Stage II
Stage III

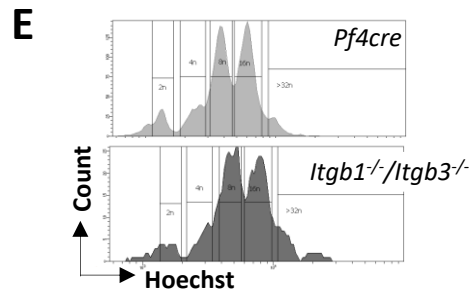
E
Pf4cre
Itgb1-/-/Itgb3-/-
Count
Hoechst

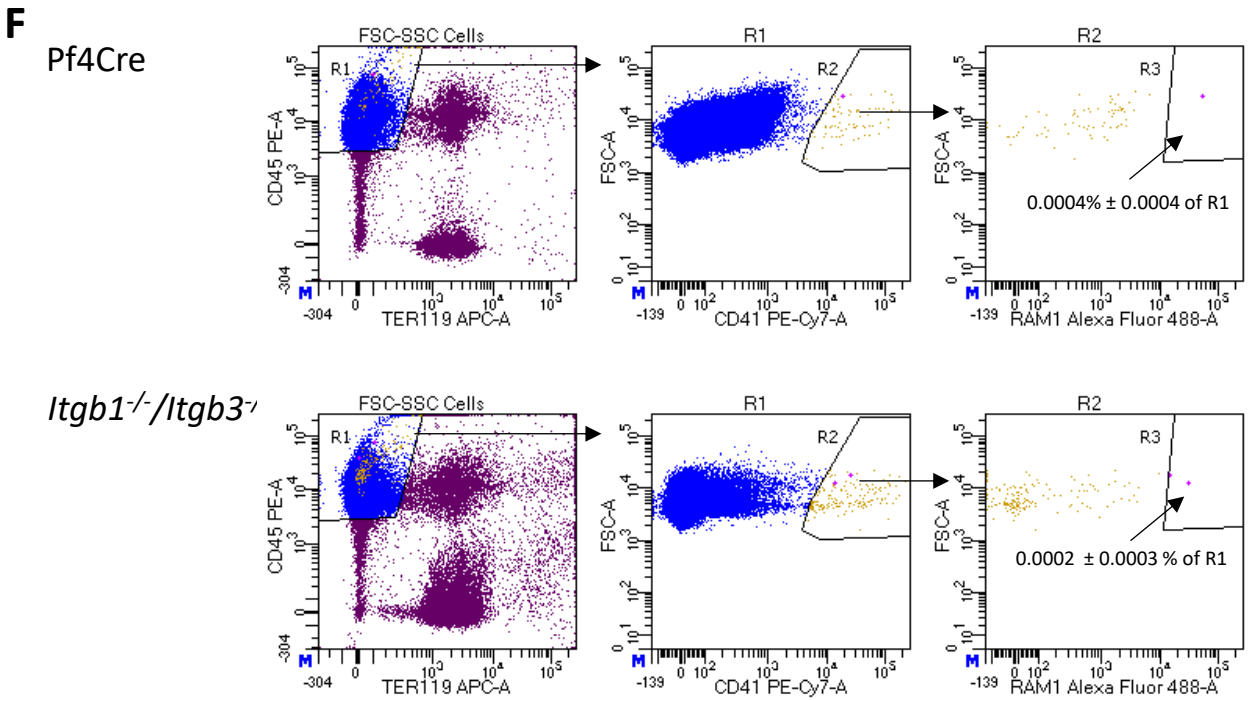
F
Pf4Cre
FSC-SSC Cells
R1
R2
R3
CD45 PE-A
TER119 APC-A
FSC-A
CD41 PE-Cy7-A
RAM1 Alexa Fluor 488-A
0.0004% ± 0.0004 of R1
Itgb1-/-/Itgb3-/-
0.0002 ± 0.0003 % of R1

Supplemental Figure 4

Characterization of *Itgb1*$^{-/-}$/*Itgb3*$^{-/-}$ platelets and megakaryocytes

(A) *Itgb1*$^{-/-}$/*Itgb3*$^{-/-}$ platelet functional properties assessed by flow cytometry.

The gating strategy was similar to that in Supplemental Figure 2B. Bar graphs showing that activated Itgb1$^{-/-}$/Itgb3$^{-/-}$ platelets expressed P-selectin but not JON-A PE. This confirmed their deficiency in integrin β3 (n=3 mice per genotype).

(B-E) Megakaryocyte density, maturation stages and ploidy were normal in *Itgb1*$^{-/-}$/*Itgb3*$^{-/-}$ bone marrow

B. Quantification of the total number of megakaryocyte, observed by electron microscopy (from 6-7 independent experiments, 120<n<153 as indicated in the bars).

C. Representative TEM images of stage III megakaryocytes. (i) The DMS is well-defined with the presence of cytoplasmic territories in control mice. (ii) In *Itgb1*$^{-/-}$/*Itgb3*$^{-/-}$ mice, the DMS accumulates in packets without marking territories (yellow arrow). Bars: 5 µm.

D. Classification of the megakaryocytes according to their maturation stage (from 3-5 independent experiments, 99<n<544).

E. Representative ploidy histograms of *Pf4cre* and *Itgb1*$^{-/-}$/*Itgb3*$^{-/-}$ megakaryocyte (one out of three independent experiments).

(F) Intact megakaryocytes were undetectable in the blood of Itgb1$^{-/-}$/Itgb3$^{-/-}$ mice.

Gating strategy for megakaryocyte identification: CD45+TER119- cells were selected from events with high FSC and SSC parameter (excluding platelets), CD41bright and CD42c bright events are megakaryocytes. The gate positions were determined based on FMO controls and biological positive controls (mouse bone marrow MK enriched cell suspension and whole blood supplemented with MK enriched cell population) (data not shown). Representative plots from 3 separate acquisitions on *Pf4cre* and *Itgb1*$^{-/-}$/*Itgb3*$^{-/-}$ mice.

A

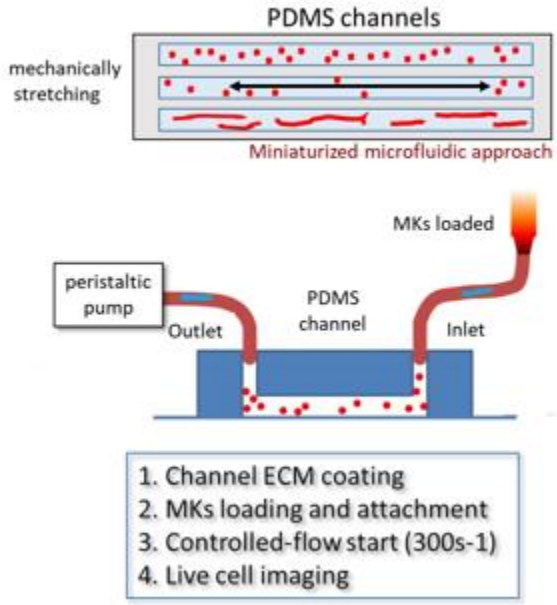

B

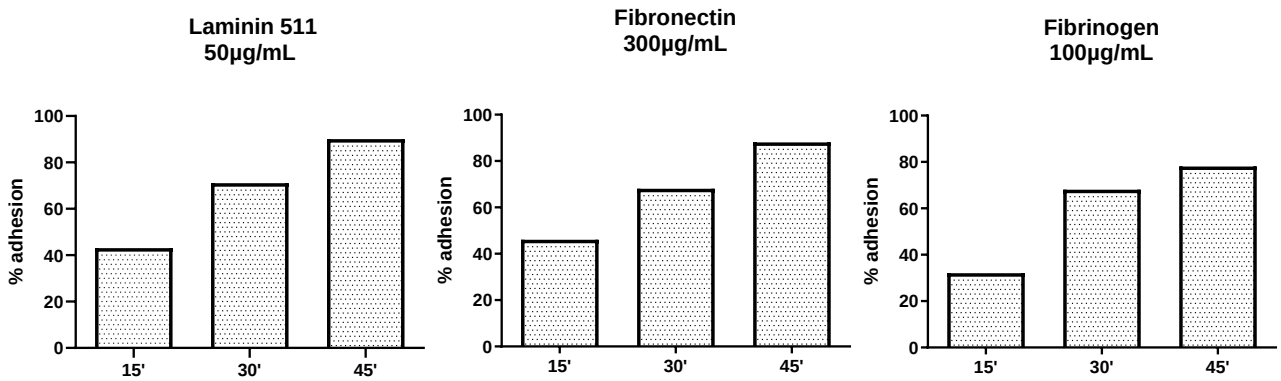

Supplement. Figure 5

Adhesive properties of *Itgb1*$^{-/-}$/*Itgb3*$^{-/-}$ megakaryocytes

(A) Schematic representation of the experimental microfluidic equipment.
(B) Determination of the seeding time with capture efficiencies of over 80 % for *Pf4cre* megakaryocytes on laminin-, fibronectin- or fibrinogen- coated chambers.

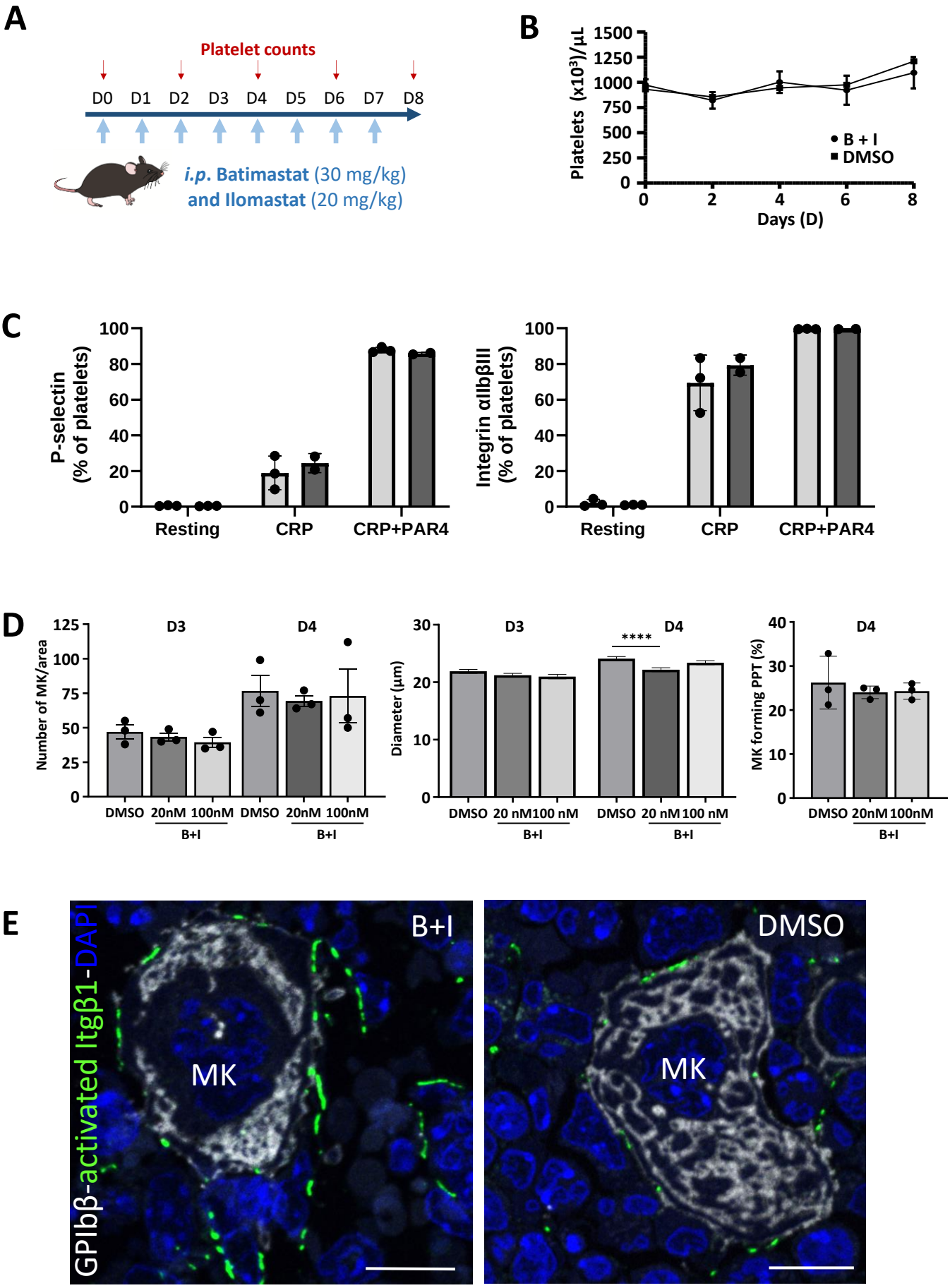
A
Platelet counts
D0 D1 D2 D3 D4 D5 D6 D7 D8
i.p. Batimastat (30 mg/kg)
and Ilomastat (20 mg/kg)
B
Platelets (x10³)/µL
1500
1250
1000
750
500
250
0
0 2 4 6 8
Days (D)
B + I
DMSO
C
P-selectin (% of platelets)
100
80
60
40
20
0
Resting
CRP
CRP+PAR4
Integrin αIIbβIII (% of platelets)
D
D3
D4
Number of MK/area
125
100
75
50
25
0
DMSO 20nM 100nM DMSO 20nM 100nM
B+I
Diameter (µm)
30
20
10
0
****
DMSO 20 nM 100 nM DMSO 20 nM 100 nM
MK forming PPT (%)
40
30
20
10
0
DMSO 20nM 100nM
E
GPIbβ-activated Itgβ1-DAPI
B+I
MK
DMSO
MK

Supplementary Figure 5

Proteolysis inhibition do not affect platelet count and *in vitro* megakaryocyte maturation.

(A) Experimental setup. A combination of batimastat (30 mg/kg) and ilomastat (20 mg/kg) (B + I) or vehicle (DMSO) was injected daily for 7 days.

(B-C) *In vivo* MMP inhibition is not impact platelet count and function.

B. Platelet counts were similar in both groups.

C. Flow cytometry shows normal P-selectin and JON-A PE expression following activation with collagen-related peptide (CRP)(40 µg/ml) or CRP + TRAP (4 mM). Bars graphs represent the percentage of positive platelets, mean ± standard error of the mean (SEM). The results were statistically compared to those of control platelets (ns, multiple unpaired t tests).

(D) *In vitro* studies demonstrate that batimastat and ilomastat have no significant direct effect on cultured megakaryocytes. This is evident from their lack of impact on : 1) proliferation (as expressed by the number of megakaryocytes (MKs) per unit), 2) maturation (as expressed by MK size in µm); 3) the ability to extend proplatelets (as expressed by the percentage of MKs that extend proplatelets). Bar graphs illustrate the impact of two MMP inhibitor doses on days 3 and 4 of the culture process, displaying the mean and standard error of the mean (SEM).

(E) Representative 2D images of bone marrow cryosections demonstrating an increase staining of activated β1 integrin (9EG7 in green) around megakaryocytes in bone marrow treated with B + I in comparison to that treated with DMSO.

*, lumen of the sinusoid; D, day; MK, megakaryocyte; Bars: 10 µm.

A. Pre-processing Workflow

(1) BM sectioning (250 µm)

(2) IF stainings

(3) z-stack for semi-MK (LAS X)

(4) Max. projection semi-MK (LAS X)

(5) Binarization (Image J)

(6) Threshold selection to reduce noise (Image J)

Step 2-4. Max. Z-stack projection around semi-MK

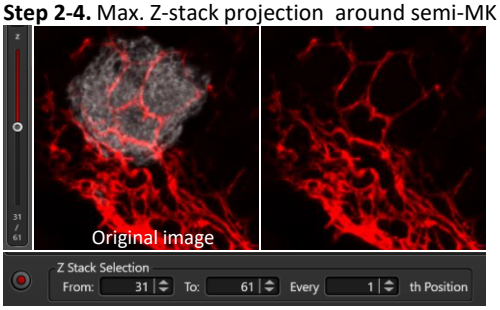

Step 5-6. Binarize

B. Features extraction

ECM coverage

(1-6) Pre-processing workflow

(7) Defining the MK ROI (Image J)

(8) ROI transfert (Image J)

(9) Tools ROI Manager : Measure

(10) Area quantification (%)

(11) Statistics
- IF experiments (n=3)
- 14 < total MK < 22

Step 7. define ROI

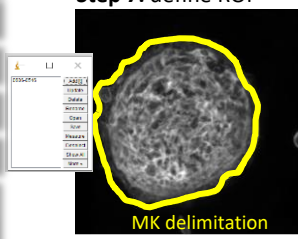

Step 8. ROI transfert

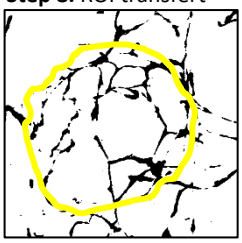

Step 10. Area quantification

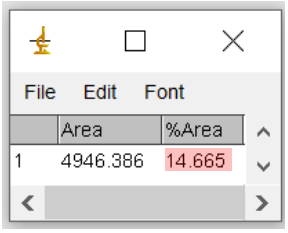

Fiber Length

(1-6) Pre-processing workflow

(7) Random length measuring
- Distance between 2 intersections points

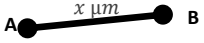

(8) Statistics
- 10 fibers/mature MK (stage 3)
- IF experiment (n=3)
- 20 < Total MK analyzed < 22

Step 7. Random length

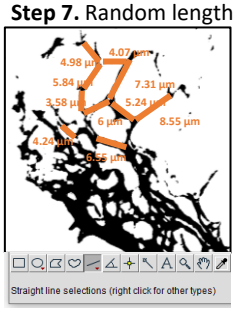

Step 8. Statistics

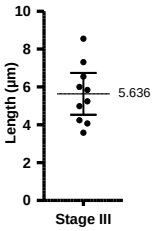

Pore Size

(1-4) Pre-processing workflow

(5) ROI : line half MK

(6) Plot profile generation

(7) Normalize data (Prism ....)
- 0%: Min value
- 100%: Max value

(8) Calculate diameter
- x position is defined by the highest peak value
- $x_{n+1} - x_n = diameter$ (µm)

(9) Statistics
- DMSO vs B+I: 7<MK<12
- PF4Cre vs Itgb1/b3: 7<MK<12

Step 5. ROI

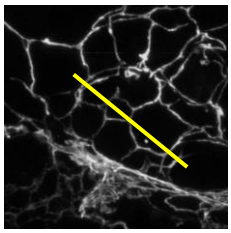

Step 6. Plot profile

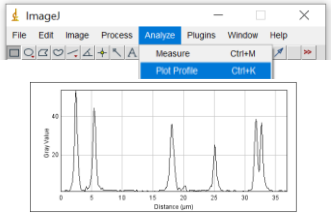

Step 7. Normalize data

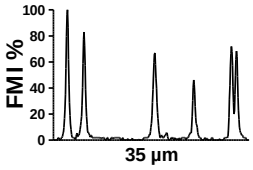

Step 8. Calculate diameter

	position (µm)
x1	1,68
x2	4,18
x3	14,56
x4	20,19
x5	25,66

	diameter (µm)
d1	2,5
d2	10,38
d3	5,63
d4	5,47

Step 9. Distribution

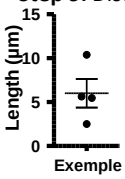

Supplementary Figure 7.
Image data flow graph

Antigen	Origin and isotype	Reference and supplier	Cryosections	Whole-mount
Primary antibody				
Collagen I	Rabbit polyclonal	Chemicon (Merck) ab765p	5µg/ml	
Collagen III		Invitrogen PA5-34787	10µg/ml	
Collagen IV		Chemicon (Merck), ab756p	5µg/ml	
FABP4	Goat polyclonal	R&D Systems AF1443	0.5µg/ml	
Fibrinogen	Rabbit polyclonal	Dako (Glostrup, Denmark), A0080	10µg/ml	
Fibronectin		ab2413 (Abcam ; Paris, France)	10µg/ml	
GPIbβ	Rat monoclonal	In house (Strasbourg, France)	1/300	1/300
Activated β1 integrin (9EG7)		553715 (BD Pharmingen)	10µg/ml	
Pan-laminin	Rabbit polyclonal	L9393 (Sigma-Aldrich)	10µg/ml	
Von Willebrand Factor		Dako, A0082	10µg/ml	
β1 integrin (MB1.2)	Rat monoclonal	Merck, MAB1997	10µg/ml	
LucA5	Rat IgG2A monoclonal	Emfret analytics, LucA5	10µg/ml	
Secondary antibody				
AF488-anti-rabbit immunoglobulin	Donkey	A21206 (Invitrogen)	1/150	
AF488-conjugated anti-rabbit immunoglobulin	Goat	A11070 (Invitrogen)		
AF647-conjugated anti-rabbit immunoglobulin	Goat	A21245 (Invitrogen)		
AF647-conjugated anti-rat immunoglobulin	Goat	A21247 (Invitrogen)		
AF555-conjugated anti-goat immunoglobulin	Donkey	A21432 (Invitrogen)		
AF647-conjugated anti-pan-laminin	Rabbit	In house	25µg/ml	
AF555-conjugated anti-collagen IV	Rabbit	In house	30µg/ml	
AF647-conjugated anti-GPIX antibody	Rat	nXiaB4 Emfret		

Table 1

Antigen	Origin and isotype	Reference and supplier	Fluorophor	Flow cytometry	Whole-mount
Conjugated antibody					
JONA Activated integrin αIIbβ3	Rat IgG2b	Emfret analytics M023-2	PE	Dilution of 1/5	
P-selectin (CD62P)	Mouse IgG2a, κ	BioLegend 148303	APC	1 µg/mL	
CD45 (clone 30-F11)	Rat IgG2b, κ	eBiosciences 12-0451-82	PE-A	1 µg/mL	
TER119	Rat / IgG2b, κ	eBiosciences 17-5921-82	APC-A	1 µg/mL	
GPIbβ	Rat monoclonal	In house (Strasbourg, France)	A647, A568, A488	1 µg/mL	
Hoechst-33342		Invitrogen H3570			10 µg/mL
Integrin αIIb (CD41 – clone MWReg30)	Rat IgG1 κ	eBiosciences 25-0411-82	PE-Cy7	1 µg/mL	

Table 2